



# Concordia

---

## MECH6161 : Gas Turbine Design Report

---

*Students :*

BHAVIK SURESHBHAI BAROT : 40234381

VALENTIN FALLOURD : 40301789

KARAN LOKHANDWALA : 40228133

SEYED MOHAMMAD NASABI : 40239558

CAMILLE PAILLARD : 40302467

JAIVYA SHAH : 40218397

*Professors :*

SAMI GIRGIS - PRATT & WHITNEY CANADA

RAJA RAMAMURTHY - PRATT & WHITNEY CANADA

TSUKASA YOSHINAKA



INSTALLATION NETWORK INC  
CRAFTING AIRBORNE EXCELLENCE

## **Abstract**

The demand for efficient and powerful gas turbine engines continues to drive innovation in the field of aerospace engineering. In response to this demand, this study presents the design and optimization of a gas turbine engine capable of producing 1150 horsepower (hp) for Pratt & Whitney engine family. We have presented this technical report to the Pratt & Whitney as a potential risk sharing partner in design and development of their new engine series. The optimization process focused on enhancing the performance of both the high-pressure turbine (HPT) and high-pressure compressor (HPC) components to achieve the desired power output while meeting stringent stage efficiency and reliability requirements.

The design process utilized advanced optimization methods implemented in Python code, leveraging mathematical modelling techniques to explore the design space and identify optimal configurations. Key parameters such as blade geometry, reaction of the turbine blades, and component materials were systematically optimized to maximize efficiency and power output while minimizing weight and operational costs.

This study also represents off-design performance of turbine and compressor blade where detailed analysis was done with reduced speed and gives a good number in efficiency of the turbine blade at off design point. Also, we have represented trade study for design of gas turbine which allow us explore design points, evaluate trade-offs, and identify optimal solutions that meet performance, cost and customer needs while managing technical risks.

Moreover. As a risk sharing partner, we have depicted our 5 Years technological business plan which shows how our organization is committed to continuous growth and future aspect with meeting all the expectations from our partners.

**Keywords:** High Pressure turbine, High Pressure compressor, Stage Efficiency, Loss Model, Hub Design, Off-design, Design optimization, Gas turbine design, Efficiency, Trade study

# Contents

<b>1</b>	<b>Introduction</b>	<b>11</b>
1.1	Project Bid . . . . .	11
<b>2</b>	<b>PART A - ENGINE DESIGN</b>	<b>12</b>
2.1	Given Data For The Calculation . . . . .	12
2.2	Cycle Calculation Assumptions . . . . .	13
2.3	Cycle Calculation . . . . .	13
2.3.1	Ambient conditions (Station process a → 01) . . . . .	14
2.3.2	Low Pressure Compressor - LPC (Station-1, Process 01 → 02) . . . . .	14
2.3.3	High Pressure Compressor - HPC (Station-2, Process 02 → 03) . . . . .	14
2.3.4	Combustor (Station-3, Process 03 → 04) . . . . .	15
2.3.5	High Pressure Turbine - HPT (Station-4, Process 04 → 05) . . . . .	15
2.3.6	Low Pressure Turbine - LPT (Station-5, Process 05 → 06) . . . . .	16
2.3.7	Power Turbine - PT (Station-6, Process 07 → 08) . . . . .	16
2.3.8	Nozzle expansion (Station-7, Process 08 → 09) . . . . .	17
<b>3</b>	<b>PART B - HPC DESIGN</b>	<b>19</b>
3.1	HPC Preliminary Design . . . . .	19
3.1.1	Introduction . . . . .	19
3.1.2	HPC Design Description . . . . .	19
3.1.3	Predicted Performance . . . . .	20
3.1.4	HPC Components . . . . .	20
3.1.5	Centrifugal Compressor Design Characteristics . . . . .	20
3.1.6	Inlet Condition . . . . .	21
3.1.7	Rotational Speed (N) and specific speed (Ns) . . . . .	21
3.2	Impeller Eye Optimization . . . . .	22
3.2.1	Inlet Hub radius . . . . .	22
3.2.2	Inlet Absolute flow swirl angle ( $\alpha_1$ ) . . . . .	24
3.2.3	Inlet Shroud radius . . . . .	25
3.2.4	Inlet Incidence Angle . . . . .	26
3.2.5	Inlet Data . . . . .	27
3.2.6	Inlet velocity Triangles . . . . .	27
3.3	Impeller Exit Optimization . . . . .	27
3.3.1	Impeller Exit Back Sweep Angle . . . . .	27
3.3.2	Exit Aerodynamic and Thermodynamics Condition at Blade Exit . . . . .	29
3.3.3	Impeller Exit Channel Height and Axial Tip Clearance . . . . .	31
3.3.4	Impeller Axial Length . . . . .	31
3.4	Vaneless Space Geometry and Diffuser Exit Design . . . . .	32

<b>4 PART C - HPT DESIGN</b>	<b>38</b>
4.1 Design Preliminary Considerations . . . . .	38
4.1.1 Given Data . . . . .	38
4.1.2 HPT Design Assumptions . . . . .	39
4.1.3 Blade Containment Considerations . . . . .	39
4.1.4 Constraints . . . . .	39
4.1.5 Radius Relations for Hub, Mean and Tip Sections . . . . .	40
4.2 Design methodology . . . . .	40
4.2.1 Velocity triangles . . . . .	40
4.2.2 Step - 1 . . . . .	40
4.2.3 Step - 2 . . . . .	41
4.2.4 Step - 3 . . . . .	41
4.2.5 Step - 4 . . . . .	42
4.2.6 Step - 5 . . . . .	43
4.2.7 Step - 6 . . . . .	43
4.2.8 Results from Off Design Analysis: . . . . .	43
4.2.9 Free vortex analysis . . . . .	45
4.2.10 Assumptions for free vortex design . . . . .	45
4.2.11 Step - 7 : Hub and Tip absolute values . . . . .	45
4.2.12 Step - 7.1 : Hub and Tip relative values . . . . .	46
4.2.13 Rsltus from Hub and Tip Line Analysis . . . . .	47
4.3 Loss Model . . . . .	48
4.3.1 Geometric Parameters . . . . .	48
4.3.2 Geometric Results . . . . .	51
4.3.3 Profile Loss . . . . .	52
4.3.4 Trailing Edge Loss . . . . .	53
4.3.5 Secondary Loss . . . . .	54
4.3.6 Total Loss . . . . .	55
4.3.7 Efficiency Calculation . . . . .	56
4.3.8 Tip Clearance Loss . . . . .	56
4.3.9 Contribution of various losses to the overall turbine efficiency . . . . .	57
4.3.10 Final Efficiency . . . . .	58
4.4 Off-Design Calculations . . . . .	58
4.4.1 Assumptions . . . . .	58
4.4.2 Calculating Incidence Angle . . . . .	58
4.4.3 Results from Mean Line Analysis . . . . .	59
4.4.4 Off-Design Profile Loss Calculations . . . . .	61
4.4.5 Off-Design Secondary Loss Calculations . . . . .	62
4.4.6 Off-Design Trailing Edge Loss Calculations . . . . .	62
4.4.7 Contribution of various losses to the overall turbine efficiency at Off-design conditions . . . . .	63
4.4.8 Off-Design Efficiency Calculations . . . . .	63
4.4.9 Stress Calculation . . . . .	64
<b>5 PART D - HPT DESIGN TRADE STUDIES</b>	<b>65</b>
5.1 Trade study of HPT factory standard cost vs. stage efficiency . . . . .	65
5.2 Engine weight reduction . . . . .	66
5.3 5 years technology plan . . . . .	68
5.4 Introducing two additional derivative engines into the market . . . . .	70

<b>6 Limitations and Conclusion</b>	<b>72</b>
6.1 Limitations . . . . .	72
6.2 Conclusion . . . . .	72

# List of Figures

2.1	Engine scheme . . . . .	12
2.2	Temperature and Pressure evolution throughout the stations . . . . .	18
2.3	Cycle Temperature vs. Entropy diagram . . . . .	18
3.1	Different compression sections [7] . . . . .	20
3.2	Centrifugal compressor mount bearing layout types [7] . . . . .	22
3.3	HPC bleed air layout [7] . . . . .	24
3.4	HPC restrictors [7] . . . . .	24
3.5	Impeller shroud relative mach number optimisation charts [7] . . . . .	25
3.6	Change in inlet relative Mach number at shroud vs. $Cx/U1m$ . . . . .	26
3.7	Impeller eye incidence angles vs. metal angles plots [7] . . . . .	26
3.8	Impeller inlet velocity triangles . . . . .	27
3.9	Pressure ratio vs. corrected tip tangential velocity ( $U_2$ ) at $\alpha$ and $\alpha_r = 0$ [7] . . . . .	28
3.10	Impeller blade exit velocity triangles [7] . . . . .	30
3.11	Graph for check for tip absolute velocity stability [7] . . . . .	30
3.12	Work loss due to change in tip clearance plots [7] . . . . .	31
3.13	Impeller span to axial length ratio visualisation [7] . . . . .	32
3.14	First diffuser leading edge velocity triangle [7] . . . . .	33
3.15	Static pressure recovery variation with block graph [7] . . . . .	34
3.16	Vanned throat incidence angle variation with block [7] . . . . .	35
3.17	Velocity triangle for vane [7] . . . . .	36
4.1	Axial gas flow . . . . .	39
4.2	Turbine velocity triangles . . . . .	40
4.3	Geometrical parameters . . . . .	49
4.4	$t_{max}/C$ vs $\beta_1 + \beta_2$ [4] . . . . .	49
4.5	Inlet Angle vs Stagger Angle [4] . . . . .	50
4.6	Blade and Vane 3D model . . . . .	52
4.7	Mounting disk 3D model and stage 3D assembly model . . . . .	52
4.8	Profile loss [3] . . . . .	53
4.9	$TETLoss \Delta\Phi_{TET}^2$ vs $t/o$ [3] . . . . .	54
4.10	Mach number correction factor K3 for the secondary loss coefficient [3] . . . . .	55
4.11	Blade losses . . . . .	57
4.12	Vane losses . . . . .	57
4.13	Effect of incidence on profile loss [4] . . . . .	61
4.14	Effect of incidence on secondary loss [4] . . . . .	62
4.15	Off-design blade losses . . . . .	63
5.1	FSC vs Stage efficiency . . . . .	66
5.2	Turbine inlet temperature effect on efficiency and weight reduction . . . . .	67
5.3	SFC vs. Turbine inlet temperature rise . . . . .	67

---

**List of Figures**

5.4	Turbine temperature inlet effect on number of blades . . . . .	67
5.5	Normalized temperature distribution curve . . . . .	68
5.6	5 years technology plan . . . . .	69

# List of Tables

1	List of symbols for overall engine . . . . .	7
2	List of locations in overall engine . . . . .	8
3	List of symbols for HPC design . . . . .	8
4	List of locations in HPC stage . . . . .	9
5	List of symbols for HPT design . . . . .	10
6	List of locations in HPT stage . . . . .	10
2.1	Engine inlet data . . . . .	12
2.2	Compressor data . . . . .	13
2.3	Combustor data . . . . .	13
2.4	Turbine data . . . . .	13
3.1	Compressor design characteristics . . . . .	21
3.2	Inlet parameters at compressor entry . . . . .	21
3.3	Incidence angles at inlet of impeller . . . . .	26
3.4	Impeller inlet parameters at different radii . . . . .	27
3.5	Variables and amounts . . . . .	29
3.6	Parameters at blade exit . . . . .	30
4.1	Stage given data . . . . .	38
4.2	Vane given data . . . . .	38
4.3	Blade given data . . . . .	38
4.4	Blade Containment Consideration . . . . .	38
4.5	Mean line analysis data . . . . .	44
4.6	Mean line analysis data . . . . .	44
4.7	Hub and Tip absolute results . . . . .	47
4.8	Hub and Tip relative results . . . . .	48
4.9	Blade Geometrical results . . . . .	51
4.10	Vane Geometrical results . . . . .	51
4.11	Mean line analysis data . . . . .	58
4.12	Mean line analysis data . . . . .	60
4.13	Mean line analysis data . . . . .	60
4.14	Other Off-design parameters at hub, mean and tip . . . . .	61
4.15	Mean line analysis data . . . . .	63
5.1	Cost of material and overhaul visits . . . . .	65
5.2	Evolution of fuel cost depending temperature rise . . . . .	68

# Nomenclature

## Overall Cycle Calculations Symbols

Symbol	Parameter Name
$P_a$	Ambient pressure ( $kPa$ )
$T_a$	Ambient temperature ( $K$ )
$P_{0i}$	Total pressure ( $kPa$ )
$T_{0i}$	Total temperature ( $K$ )
$\Delta P_0$	Pressure loss/drop ( $kPa$ )
$\dot{m}_i$	Mass flow rate ( $kg/s$ )
$PR_i$	Pressure ratio
$\eta_i$	Component efficiency (%)
$f$	Fuel to air ratio
$LHV$	Lower heating value ( $kJ/kg$ )
$\dot{m}_f$	Mass flow rate of fuel ( $kg/s$ )
$Cp_a$	Specific heat value for air ( $kJ/kgK$ )
$Cp_g$	Specific heat value for gas ( $kJ/kgK$ )
$\gamma$	Specific heat ratio
$W_i$	Work done/consumed ( $kW$ )
$M_e$	Exhaust Mach number
$SFC$	Specific fuel consumption ( $kg/kWh$ )
subscript $i$	Location in the overall engine

Table 1: List of symbols for overall engine

Subscript $i$	Location
$a$	Intake
01	Low pressure compressor inlet
02	High pressure compressor inlet
03	Combustor inlet
04	High pressure turbine inlet
05	Low pressure turbine inlet
06	Intermediate turbine duct inlet
07	Power turbine inlet
08	Exhaust inlet
09	Exhaust Exit
$LPC$	Low Pressure Compressor
$HPC$	High Pressure Compressor
$HPT$	High Pressure Turbine

Subscript $i$	Location
$LPT$	Low Pressure Turbine
$PT$	Power Turbine

Table 2: List of locations in overall engine

## High Pressure Centrifugal Compressor Design Symbols

Symbol	Parameter Name
$N_s$	Specific speed
$N$	RPM
$\alpha_i$	Absolute flow angle(deg)
$\beta_i$	Rlative flow angle (deg)
$\beta_i^*$	Blade angle (deg)
$N_b$	Number of blades
$\eta$	Total to total efficiency
$\dot{m}_i$	Mass flow rate ( $kg/s$ )
$T_i$	Static temperature ( $K$ )
$T_{0i}$	Total temperature ( $K$ )
$P_i$	Static pressure ( $kPa$ )
$\rho_{0i}$	Total density ( $kg/m^3$ )
$\rho_i$	Density ( $kg/m^3$ )
$Q$	Volumetric flow rate ( $m^3/s$ )
$R$	Universal gas constant ( $J/kgK$ )
$\Delta h_{0,is}$	Total isentropic enthalpy ( $kJ/kgK$ )
$C_i$	Absolute velocity ( $m/s$ )
$C_{xi}$	Absolute axial velocity ( $m/s$ )
$W_i$	Relative velocity ( $m/s$ )
$U_i$	Rotational Speed ( $m/s$ )
$A_i$	Area ( $mm^2$ )
$\sigma$	Aerodynamic slip factor
$b_i$	blade exit channel height ( $mm$ )
$M_{iabs}$	Absolute Mach number
$M_{irel}$	Relative Mach number
$r_i$	Radius ( $mm$ )
$h_{0i}$	Total enthalpy ( $kJ/kgK$ )
$\gamma$	Specific heat ratio
$\phi$	Diffusion Angle (deg)
$\omega$	Diffuser wedge angle (deg)
$N_v$	Diffuser Vane Count
$N_b$	Diffuser blade count

Table 3: List of symbols for HPC design

Subscript $i$	Location
1	Impeller Inlet
2	Impeller Exit
3	Diffuser Leading Edge
*	Diffuser Throat
5	HPC exit
$h$	At hub radius
$m$	At mean radius
$sh$	At shroud radius

Table 4: List of locations in HPC stage

## High Pressure Turbine Design Symbols

Symbol	Parameter Name
$A_j$	Area ( $mm^2$ )
$P_{0j}$	Total pressure ( $kPa$ )
$P_{0jr}$	Relative total pressure ( $kPa$ )
$N$	RPM
$t_{te,j}$	Trailing edge thickness ( $mm$ )
$r_j$	Radius ( $mm$ )
$\dot{m}_j$	Mass flow rate ( $kg/s$ )
$\dot{m}_a$	Mass flow rate of air ( $kg/s$ )
$\dot{m}_f$	Mass flow rate of fuel ( $kg/s$ )
$T_j$	Static temperature ( $K$ )
$T_{0j}$	Total temperature ( $K$ )
$T_{0jr}$	Relative total temperature ( $K$ )
$P_j$	Static pressure ( $kPa$ )
$\rho_j$	Density ( $kg/m^3$ )
$\gamma_g$	Specific heat ratio
$R_g$	Universal gas constant ( $J/kgK$ )
$C_j$	Absolute velocity ( $m/s$ )
$C_{aj}$	Absolute axial velocity ( $m/s$ )
$C_{wj}$	Absolute tangential velocity ( $m/s$ )
$R_j$	Temperature based reaction
$M_j$	Absolute Mach number
$U_j$	Blade tangential velocity ( $m/s$ )
$\omega$	Blade Angular velocity ( $rad/s$ )
$h_j$	height ( $mm$ )
$V_j$	Relative velocity ( $m/s$ )
$V_{wj}$	Relative tangential velocity ( $m/s$ )
$M_{rj}$	Relative Mach number
$r_j$	Radius ( $mm$ )
$\alpha_j$	Absolute flow angle ( $deg$ )
$\alpha_{jr}$	Relative flow angle ( $deg$ )
$\beta_j$	Metal angle ( $deg$ )
$h_{0j}$	Total enthalpy ( $kJ/kgK$ )
$AR_j$	Aspect ratio

<b>Symbol</b>	<b>Parameter Name</b>
$C_j$	Chord length ( $mm$ )
$t_{max,j}$	Maximum thickness ( $mm$ )
$C_{a,j}$	Axial Chord length ( $mm$ )
$\phi_j$	Stagger angle ( $deg$ )
$\psi_j$	Zweifel coefficient
$N_j$	Number of airfoils
$K_k$	Loss coefficient
$Re$	Reynolds number
$\zeta_j$	Pressure loss coefficient
$\eta_{tt}$	Total to total stage efficiency (%)
$W_j$	Work ( $Watts$ )
Subscript $j$	Location relative to HPT stage
Subscript $i$	Incidence
Subscript $k$	Type of loss

Table 5: List of symbols for HPT design

<b>Subscript <math>i</math></b>	<b>Location</b>
1	Inlet of guide vane/stator
2	Outlet of guide vane/stator or inlet of blade/rotor
3	Outlet of blade/rotor
$h$	At hub radius
$m$	At mean radius
$t$	At tip radius

Table 6: List of locations in HPT stage

# Chapter 1

## Introduction

Finding powerful and efficient gas turbine engines is a key component of innovation in the ever-changing field of aeronautical engineering. This study sets out to design and optimize a gas turbine engine that can produce 1150 horsepower (hp), specifically for the prestigious Pratt & Whitney engine family, in response to the growing need for high-performance propulsion systems.

Motivated by the need to improve performance, we are working to submit a technical report to Pratt & Whitney that outlines our potential partnership as a risk-sharing partner for the design and development of their upcoming engine series. The high-pressure turbine (HPT) and high-pressure compressor (HPC) components are the keystones of our optimization technique. They are carefully tuned to produce the desired power output while meeting strict stage efficiency and reliability standards.

### 1.1 Project Bid

The project entails the design, optimization, and manufacturing of key rotating components, including high-pressure turbine (HPT) and high-pressure compressor (HPC) parts, for Pratt & Whitney's next-generation gas turbine engine. As a risk-sharing partner, our role will be to collaborate closely with Pratt & Whitney's engineering team to ensure the successful realization of the engine's performance objectives while managing technical risks.

## Chapter 2

# PART A - ENGINE DESIGN

### 2.1 Given Data For The Calculation

The different layouts of the engine to design are as follows :

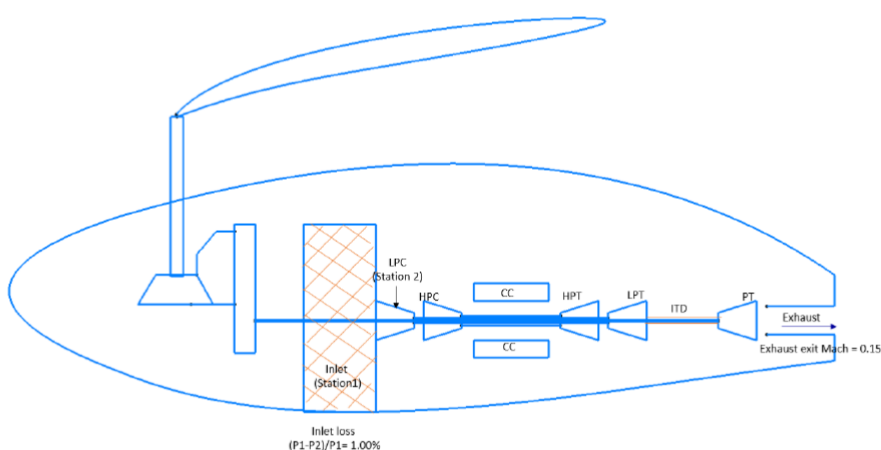


Figure 2.1: Engine scheme

From this point, data are provided to perform the cycle calculation at the various engine stations.

Parameter Name	Symbol	Value
Ambient Pressure	Pa	101.235 kPa
Ambient Temperature	Ta	296.48 K
Engine Inlet Total Pressure Loss	$\Delta P_0$	1 %

Table 2.1: Engine inlet data

Parameter Name	Symbol	Value
Mass Flow	$\dot{m}$	5.2163 kg/s
Low Pressure Combustor Pressure Ratio	$PR_{LPC}$	4
Low Pressure Compressor Target Efficiency	$\eta_{LPC}$	86.5 %
High Pressure Combustor Pressure Ratio	$PR_{HPC}$	3
High Pressure Compressor Target Efficiency	$\eta_{HPC}$	85.5 %
Bleed air taken at HPC exit (cabin bleed + turbine cooling)	$\dot{m}_{a,bleeded}$	9 % of inlet flow

Table 2.2: Compressor data

Parameter Name	Symbol	Value
Fuel to air ratio	$f$	0.02
Heating value	$LHV$	17200 BTU/lb = 40007.2 kJ/kg
Combustor efficiency	$\eta_{combustor}$	99%
Total Pressure loss	$\Delta P_0$	1.8%

Table 2.3: Combustor data

Parameter Name	Symbol	Value
High Pressure Turbine target efficiency	$\eta_{HPT}$	83%-85%
High Pressure Turbine vane cooling air	$\dot{m}_v$	3% of $\dot{m}_{a,bleeded}$
High Pressure Turbine disk cooling air	$\dot{m}_d$	1.65% of $\dot{m}_{a,bleeded}$
Low Pressure Turbine target efficiency	$\eta_{LPT}$	91%
Low Pressure Turbine disk cooling air	$\dot{m}_{d2}$	1.1% of $\dot{m}_d + \dot{m}_{g2}$
ITD Total Pressure loss	$\Delta P_0$	0.6%
Pressure Turbine target efficiency	$\eta_{PT}$	92%
Power Turbine disk cooling air	$\dot{m}_{g4}$	1.25% of $\dot{m}_{g3}$
Exhaust Total Pressure loss	$\Delta P_0$	2%
Exhaust exit Mach number	$M_e$	0.15

Table 2.4: Turbine data

## 2.2 Cycle Calculation Assumptions

Several assumptions were necessary to perform the cycle calculation based on the given data :

- Assume atmospheric air as a working medium until combustor section.  
Thus,  $C_P = 1.005 \text{ kJ/kg}$  and  $\gamma = 1.4$
- Combustion gases are considered as working fluid in the rest of the engine.  
Thus,  $C_P = 1.148 \text{ kJ/kg}$  and  $\gamma = 1.33$
- Mechanical efficiencies ( $\eta_m$ ) for high and low pressure turbomachines is 99%
- High Pressure Turbine target efficiency is assumed to be 84%

## 2.3 Cycle Calculation

### 2.3.1 Ambient conditions (Station process a → 01)

$$Pa = 101.235 \text{ kPa}$$

$$Ta = T_{01} = 296.48 \text{ K}$$

$$P_{01} = 100.306 \text{ kPa}$$

$$\dot{m} = 5.2163 \text{ kg/s}$$

### 2.3.2 Low Pressure Compressor - LPC (Station-1, Process 01 → 02)

$$P_{02} = 4 * P_{01} = 4 * 100.306 = 401.224 \text{ kPa}$$

$$\left(\frac{P_{02}}{P_{01}}\right)^{\frac{\gamma-1}{\gamma}} = \frac{T_{02}}{T_{01}}$$

$$T_{02i} = 440.56 \text{ K}$$

$$\eta_{LPC} = \frac{T_{02i} - T_{01}}{T_{02} - T_{01}}$$

$$T_{02} = 463.046 \text{ K}$$

$$W_{LPC} = \dot{m}Cp_a(T_{02} - T_{01}) = 5.2163 * 1.005 * (463.046 - 296.48) = 873.47 \text{ kW}$$

### 2.3.3 High Pressure Compressor - HPC (Station-2, Process 02 → 03)

$$P_{03} = 3 * P_{02} = 3 * 401.224 = 1203.672 \text{ kPa}$$

$$\left(\frac{P_{03}}{P_{02}}\right)^{\frac{\gamma-1}{\gamma}} = \frac{T_{03}}{T_{02}}$$

$$T_{03i} = 633.79 \text{ K}$$

$$\eta_{HPC} = \frac{T_{03i} - T_{02}}{T_{03} - T_{02}}$$

$$T_{03} = 662.75 \text{ K}$$

$$W_{HPC} = \dot{m}Cp_a(T_{03} - T_{02}) = 5.2163 * 1.005 * (662.75 - 463.046) = 1046.925 \text{ kW}$$

### 2.3.4 Combustor (Station-3, Process 03 → 04)

$$\dot{m}_{a,bleeded} = 5.2163 * 0.91 = 4.7468 \text{ kg/s}$$

$$\frac{\dot{m}_f}{\dot{m}_a} = f = 0.02$$

$$\dot{m}_f = 0.02 * \dot{m}_a = 0.02 * 4.7468 = 0.0949 \text{ kg/s}$$

$$P_{04} = P_{03} * 0.982 = 1203.672 * 0.982 = 1182.006 \text{ kPa}$$

$$Q = E_{out} - E_{in} \Leftrightarrow \dot{m}_f * LHV + \dot{m}_a C_{P_a} T_{03} = (\dot{m}_a + \dot{m}_f) C_{P_g} T_{04}$$

$$T_{04} = 1251.890 \text{ K}$$

### 2.3.5 High Pressure Turbine - HPT (Station-4, Process 04 → 05)

Calculate turbine mass flow rate :

$$\dot{m}_{g1} = \dot{m}_{a,bleeded} + \dot{m}_f = 4.7468 + 0.0949 = 4.8417 \text{ kg/s}$$

$$\dot{m}_v = \dot{m}_{a,bleeded} * 0.03 = 4.7468 * 0.03 = 0.1424 \text{ kg/s}$$

$$\dot{m}_d = \dot{m}_{a,bleeded} * 0.0165 = 4.7468 * 0.0165 = 0.07832 \text{ kg/s}$$

Vane balance :

$$\dot{m}_{g1} C_{p_g} T_{04} + \dot{m}_v C_{p_a} T_{03} = (\dot{m}_{g1} + \dot{m}_v) C_{p_g} T_{04a} \Leftrightarrow T_{04a} = 1232.70 \text{ K}$$

$$\eta_m = \frac{W_{HPC}}{W_{HPT}} \Leftrightarrow W_{HPT} = \frac{W_{HPC}}{\eta_m} = \frac{1046.925}{0.99} = 1057.5 \text{ kW}$$

$$\dot{m}_{g2} = \dot{m}_{g1} + \dot{m}_v = 4.8417 + 0.1424 = 4.9841 \text{ kg/s}$$

$$W_{HPT} = (\dot{m}_{g2} + \dot{m}_d) C_{p_g} (T_{04a} - T_{05}) \Leftrightarrow T_{05} = 1050.74 \text{ K}$$

$$\frac{P_{05}}{P_{04}} = \left[ 1 - \frac{1}{\eta_{HPT}} * \left( 1 - \frac{T_{05}}{T_{04}} \right) \right]^{\frac{\gamma}{\gamma-1}} \Leftrightarrow \boxed{P_{05} = 542.45 \text{ kPa}}$$

Blade balance :

$$\dot{m}_{g3} = \dot{m}_{g2} + \dot{m}_v = 4.9841 + 0.1424 = 5.1265 \text{ kg/s}$$

$$\dot{m}_{g2}Cp_gT_{05} + \dot{m}_dCp_aT_{03} = (\dot{m}_{g2} + \dot{m}_d)Cp_gT_{05b} \Leftrightarrow T_{05b} = 1043.46 \text{ K}$$

### 2.3.6 Low Pressure Turbine - LPT (Station-5, Process 05 → 06)

$$\dot{m}_{g3} = \dot{m}_{g3} + \dot{m}_d = 5.1265 + 0.07832 = 5.2049 \text{ kg/s}$$

$$\dot{m}_{d2} = 0.011 * (\dot{m}_d + \dot{m}_{g2}) = 0.011 * (0.07832 + 4.9841) = 0.05569 \text{ kg/s}$$

$$\eta_m = \frac{W_{LPC}}{W_{LPT}} \Leftrightarrow \boxed{W_{LPT} = \frac{W_{LPC}}{\eta_m} = \frac{873.47}{0.99} = 882.29 \text{ kW}}$$

$$W_{LPT} = (\dot{m}_{g3} + \dot{m}_{d2})Cp_g(T_{05b} - T_{06}) \Leftrightarrow \boxed{T_{06} = 897.36 \text{ K}}$$

$$\frac{P_{06}}{P_{05}} = \left[ 1 - \frac{1}{\eta_{LPT}} * \left( 1 - \frac{T_{06}}{T_{05}} \right) \right]^{\frac{\gamma}{\gamma-1}} \Leftrightarrow \boxed{P_{06} = 268.12 \text{ kPa}}$$

$$\dot{m}_{g3}Cp_gT_{06} + \dot{m}_{d2}Cp_aT_{03} = (\dot{m}_{g3} + \dot{m}_{d2})Cp_gT_{06a} \Leftrightarrow T_{06a} = 894 \text{ K}$$

### 2.3.7 Power Turbine - PT (Station-6, Process 07 → 08)

$$\boxed{Itd \ loss = P_{07} = P_{06} * (1 - 0.006) = 266.51 \text{ kPa}}$$

$$\boxed{T_{07} = T_{06a} = 894 \text{ K}}$$

$$M_{g4} = \dot{m}_{g3} - 0.0125 * \dot{m}_{g3} = 5.1398 \text{ kg/s}$$

### 2.3.8 Nozzle expansion (Station-7, Process 08 → 09)

$$\frac{P_9}{P_{09}} = \left[ 1 + \left( \frac{\gamma - 1}{2} \right) M e^2 \right]^{\frac{-\gamma}{\gamma-1}} \Leftrightarrow [P_{09} = 102.85 \text{ kPa}]$$

Considering 2% pressure loss in the nozzle :

$$[P_{08} = 1.02 * P_{09} = 104.91 \text{ kPa}]$$

Going back to power turbine (Process 07 → 08) :

$$\frac{P_{08}}{P_{07}} = \left( \frac{T_{08a}}{T_{07}} \right)^{\frac{\gamma}{\gamma-1}} \Leftrightarrow T_{08a} = 709.37 \text{ K}$$

Considering turbine efficiency :

$$\eta_t = \frac{T_{07} - T_{08}}{T_{07} - T_{08a}} \Leftrightarrow [T_{08} = 724.14 \text{ K}]$$

Shaft power is given by :

$$[W_{PT} = \dot{m}_{g4} C p_g (T_{07} - T_{08}) \eta_m = 992.27 \text{ kW}]$$

Finally, Specific Fuel Consumption (SFC) is given by :

$$[SFC = \frac{3600 * f}{\frac{W_{PT}}{\dot{m}_{g4}}} = \frac{3600 * 0.02}{193.06} = 0.3728 \text{ kg/kWh}]$$

Thus, one can visualize the evolution of the temperature and the pressure throughout the different stations of the engine :

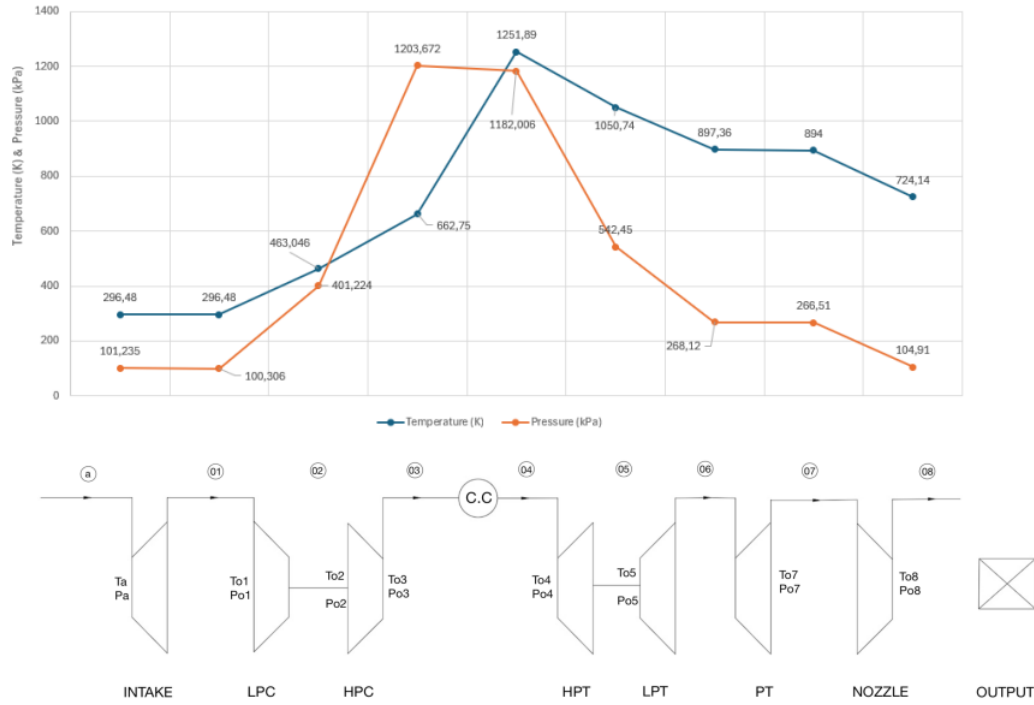


Figure 2.2: Temperature and Pressure evolution throughout the stations

This also results in the following cycle Temperature vs. Entropy diagram :

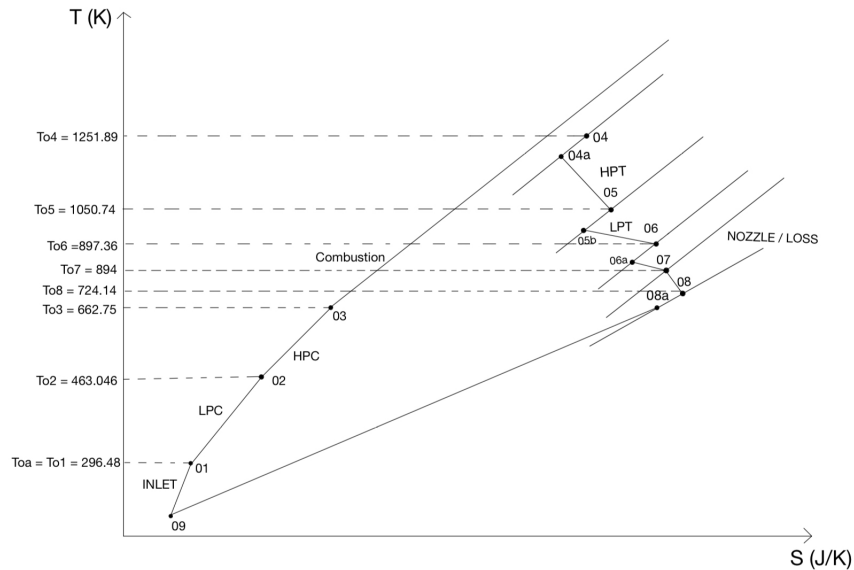


Figure 2.3: Cycle Temperature vs. Entropy diagram

# Chapter 3

## PART B - HPC DESIGN

### 3.1 HPC Preliminary Design

#### 3.1.1 Introduction

In this chapter, the goal is to find the Centrifugal High-Pressure Compressor parameters with respect to the given data and a compromise with High Pressure Turbine. A centrifugal compressor is a type of dynamic compressor that utilizes the kinetic energy of a rotating impeller to increase the pressure and density of a gas or air stream. The basic principle behind a centrifugal compressor involves drawing in a gas through an inlet, where it is accelerated by the high-speed rotation of the impeller. As the gas moves outward and encounters the curved blades of the impeller, its velocity is converted into pressure energy, resulting in a higher pressure at the compressor outlet. Centrifugal compressors are known for their compact design, high efficiency, and ability to handle large volumes of gas at relatively low compression ratios. They are often preferred for applications requiring continuous, steady flow rates and where space constraints are a concern.

#### 3.1.2 HPC Design Description

The High pressure compressor which has been designed in the present case is a centrifugal type compressor with following sections :

- Impeller
- Vane-less Diffuser
- Primary Vaned Diffuser

The design specifications for the high-pressure centrifugal compressor(HPC) include :

- Operating centrifugal specific speed set at 70.27.
- Inlet flow configured to create a swirl angle of 20 degrees with axial direction.
- The specific speed is chosen to ensure that the HPC rotor RPM matches the HPT rotor RPM.
- An optimal specific speed is selected to minimize total loss coefficients.

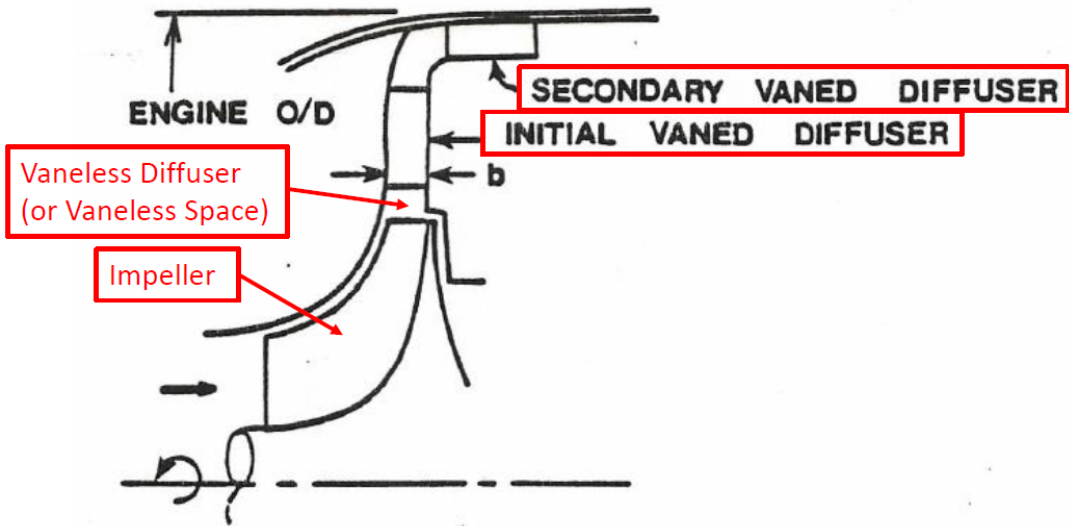


Figure 3.1: Different compression sections [7]

### 3.1.3 Predicted Performance

#### *Pressure Ratio*

The total to total pressure ratio for the current HPC is 3.

#### *Efficiency*

A total to static efficiency of 85.5 % between the impeller inlet and diffuser is considered in the present design and an adiabatic efficiency of 88.5 % is considered for impeller.

### 3.1.4 HPC Components

The centrifugal compressor consists of two primary components :

- Impeller
  - Impeller Eye
  - Impeller tip section
- Diffuser
  - Pipe Section
  - Vaned Diffuser throat section

Properly labeling these sections of the compressor facilitates easy recognition during calculations.

### 3.1.5 Centrifugal Compressor Design Characteristics

The design characteristics of the compressor (both implicit and explicit) are described below :

Stage		
Characteristics	Sub-Characteristics	Value/Range
Specific Speed ( $N_s$ )		55 – 85
Impeller	Inlet Swirl ( $\alpha_1$ ) Impeller Exit Back Sweep ( $\beta_2^*$ ) Number of blades ( $N_b$ ) Impeller Adiabatic Efficiency ( $\eta$ )	5° – 35° –40° – 0° 16 full and 16 splitter 88.5%
Diffuser	Chocke Margin Throat Aspect Ratio	1.25% 0.8-1.2
Others	RPM Target Efficiency (Total to Static) Pressure Ratio Meridional Velocity Ratio	35,000 85.5% 3 0.8 – 1

Table 3.1: Compressor design characteristics

### 3.1.6 Inlet Condition

The flow before entering the HPC passes through the Low-Pressure Compressor and the pressure is increased by the pressure ratio of LPC. In order to calculate the parameters through HPC, it is necessary to know about the initial conditions at HPC entrance. Here, a table of given data and calculated data is provided :

Variable	Amount	Variable	Amount
$P_{01}$	401.224 kPa	$T_{01i}$	440.56 K
$P_{05}$	1203.672 kPa	$T_{05i}$	633.79 K
$T_{01}$	463.046 K	Mass Flow Rate( $\dot{m}_1$ )	5.2163 kg/s
$T_{05}$	662.75 K	Target Efficiency	85.5%
$N_s$	55-85	$\alpha_1$	5° – 35°
Adiabatic Efficiency	88.5%	Number of Blades	32
		$\beta_2^*$	–40° – 0°

Table 3.2: Inlet parameters at compressor entry

### 3.1.7 Rotational Speed (N) and specific speed ( $N_s$ )

In order to start the calculation regarding the inlet of HPC, a compromise with the HPT group should be done to find a rotational speed for the common shaft of HPC and HPT. The process starts from obtaining data from HPT group and using them as initial guess for HPC calculations to find the best parameters that satisfy the assigned conditions. This compromise is done and a rotational speed ( $N$ ) of 35000 RPM is used for the calculation. The corresponding specific speed ( $N_s$ ) is obtained through the following formula :

$$N_s = \frac{N\sqrt{Q_1}}{(778.26 \times \Delta h_{0,is})^{0.75}}$$

$$Q_1 = \frac{\dot{m}_1}{\rho_1}$$

$$\rho_{01} = \frac{P_{01} \times R}{T_{01}}$$

In which  $\Delta h_{0,is}$  is the total isentropic enthalpy rise by the HPC and  $Q_1$  is the volumetric flow rate. In the first step, total density is used for calculating volumetric flow rate. Later, through an iterative process static density, the corresponding volumetric flow rate and specific speed is corrected. The obtained specific speed is between the range and is acceptable.

## 3.2 Impeller Eye Optimization

### 3.2.1 Inlet Hub radius

The hub radius of HPC is obtained through a ratio-ing HPT rotor gas path hub radius. A ratio of 0.75 is assigned for the ratio between inlet HPC hub radius over HPT hub radius.

$$\frac{r_{1h \text{ HPC}}}{r_{1h \text{ HPT}}} = 0.75$$

$$r_{1h \text{ HPC}} = 0.06357 \text{ m}$$

Regarding the non-aero design requirement of the HPC inlet hub radius, by increasing the inlet hub radius the overall centrifugal compressor would have a large dimension which is not favorable from design point of view. On the other hand, smaller diameter for inlet hub radius is controlled by mechanical and structural requirements.

#### Factors that Affect the Calculation of Hub Radius ( $r_{hub}$ )

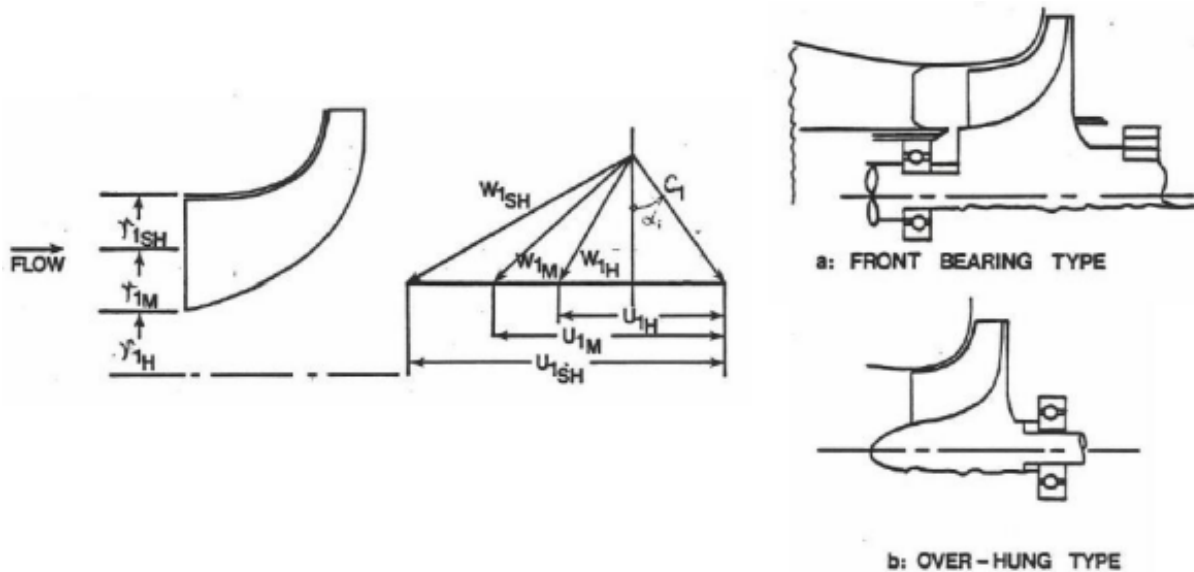


Figure 3.2: Centrifugal compressor mount bearing layout types [7]

#### Structural Requirement (Max Turbine Rim Speed)

At a constant rotational speed (RPM), the radius of the turbine hub is limited by the maximum allowable turbine rim speed due to centrifugal stress. This limitation indirectly affects the compressor hub radius. The relationship between these parameters is expressed by the following equation :

$$U_h = 2\pi \left( \frac{N_{rpm}}{60} \right) r_h$$

### **Combined Structural and Aerodynamic Requirements**

The design of a turbine and compressor system involves balancing both structural and aerodynamic considerations. Centrifugal Stress and Turbine Geometry. Turbine blades experience significant centrifugal stress ( $\sigma_{max}$ ) due to their rotation at high speeds. This stress is limited to a maximum value ( $\sigma_{max,allowable}$ ). The relationship between centrifugal stress, tip rotational speed ( $U_{tip}$ ), hub radius ( $r_{hub}$ ), and tip radius ( $r_{tip}$ ) is expressed by the following equation :

$$\sigma_{max} = \rho \frac{U_{sh}^2}{2} \left( 1 - \frac{r_h^2}{r_{sh}^2} \right)$$

This equation shows that for a fixed maximum stress, there's a trade-off between tip speed and the ratio of hub radius to tip radius. A higher tip speed necessitates a larger hub-to-tip ratio to keep the stress within limits. Additionally, a maximum allowable tip rotational speed can be derived from the stress equation and used to determine the tip radius through the following expression :

$$U_{sh} = \sqrt{\frac{2\sigma_{max,allowable}}{\rho} \left( 1 - \frac{r_h^2}{(r_{sh})^2} \right)} \quad (\text{fixed tip radius})$$

This equation highlights that with a fixed tip radius, a larger hub radius leads to a lower allowable tip speed to maintain structural integrity.

### **Airflow Requirements and Hub Radius**

To achieve a desired mass flow rate ( $\dot{m}$ ) and maintain the continuity equation, a specific flow area (A) is required in the turbine. This area is calculated using the following relationship :

$$A = \frac{\dot{m}}{\rho C_a}$$

The flow area can also be expressed in terms of the hub and tip radii :

$$A = \pi(r_{sh}^2 - r_h^2)$$

Combining these two equations allows us to determine the required hub radius based on the desired mass flow rate and other parameters. Consequently, setting the turbine hub radius indirectly sets the compressor hub radius as well (assuming a fixed ratio between them). In conclusion, designing a turbine and compressor system involves finding an optimal balance between structural limitations imposed by centrifugal stress and aerodynamic requirements for airflow. This balance dictates the choice of hub and tip radii, ultimately affecting the overall performance and efficiency of the system.

### **Mechanical Requirement**

The layout of centrifugal compressor mount affects hub radius and on the other hand, the layout mount is affected by factors like :

- The air bleed piping system layout.
- The mechanical seals and restrictors needed to control bleed air flow.

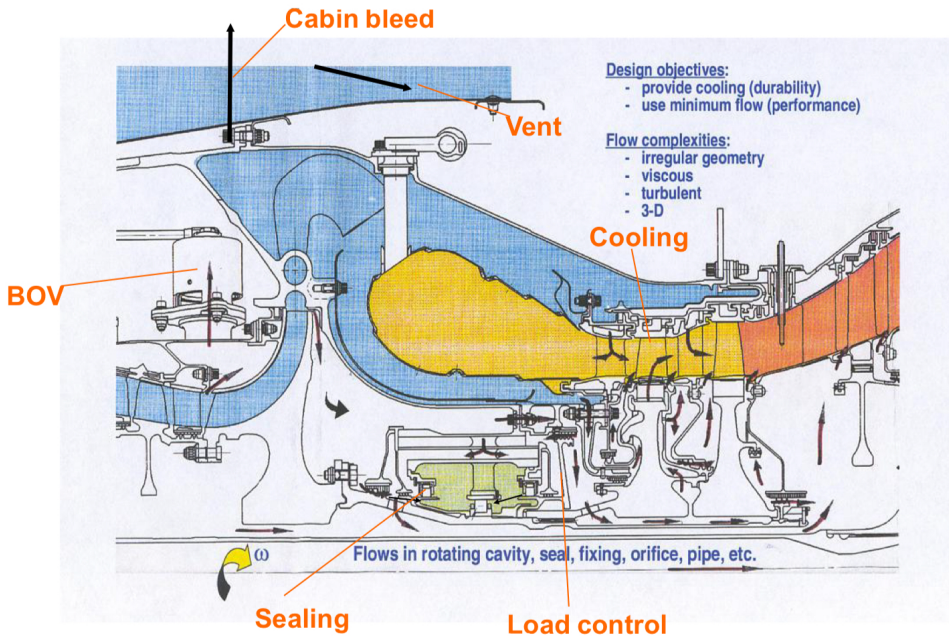


Figure 3.3: HPC bleed air layout [7]

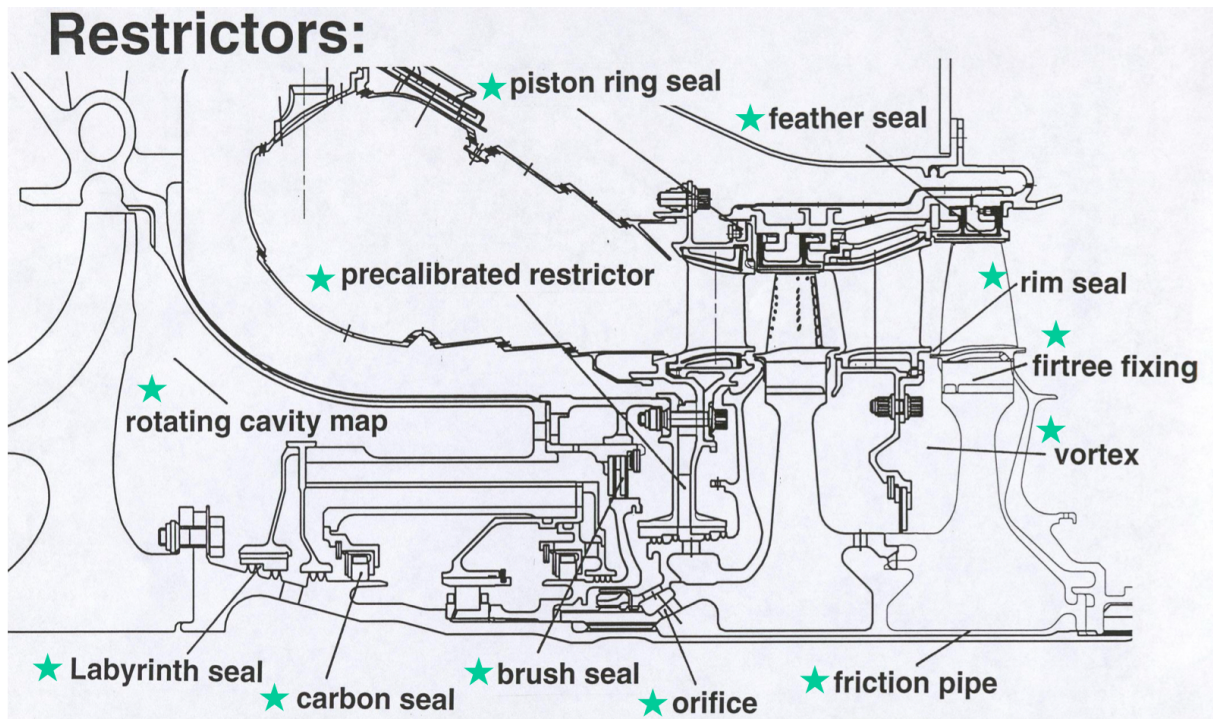


Figure 3.4: HPC restrictors [7]

### 3.2.2 Inlet Absolute flow swirl angle ( $\alpha_1$ )

Absolute flow swirl angle indicates how the flow enters the compressor; this angle can define the relative velocity by knowing the rotational speed ( $U$ ). For this project,  $\alpha_1$  is assumed to be 20 degrees.

### 3.2.3 Inlet Shroud radius

Optimizing the design of the impeller eye in a centrifugal compressor involves balancing two key considerations :

- **Static Density** : The static density of the working fluid plays a crucial role in the performance of the impeller. Optimizing the geometry of the impeller eye aims to achieve a desired distribution of static density within the flow path.
- **Minimum Shroud Relative Mach Number** : Another critical factor is minimizing the relative Mach number at the impeller shroud. This minimization helps to reduce compressibility effects and potential losses at the impeller shroud.

Finding an optimal design for the impeller eye involves considering both static density distribution and minimizing the relative Mach number at the shroud. This balance ensures efficient flow through the impeller while minimizing compressibility losses.

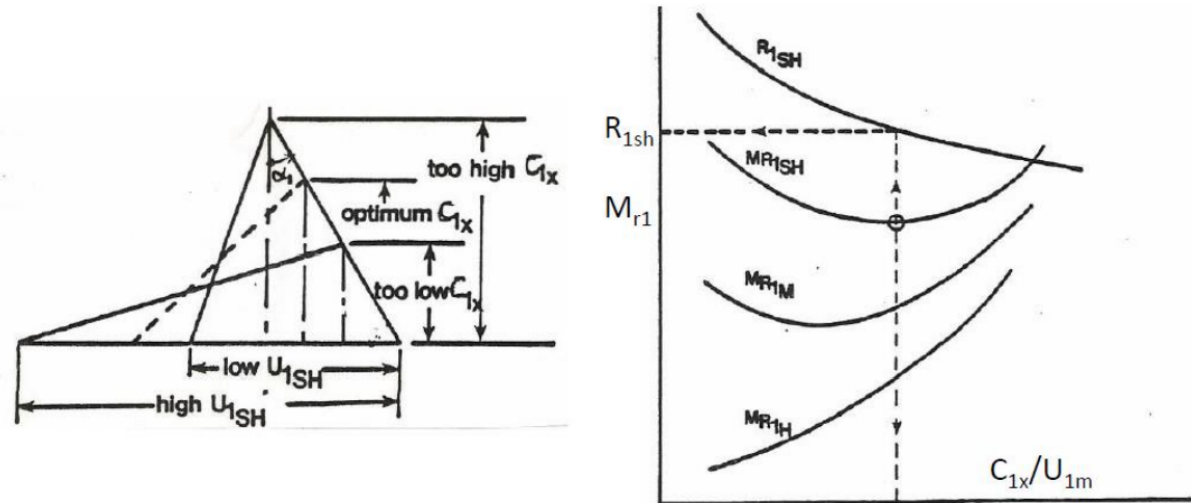


Figure 3.5: Impeller shroud relative mach number optimisation charts [7]

For the shroud radius, the criteria that are significant is that the relative Mach number which obtains from relative velocity is the lowest. The process is done through an iterative loop for a range of Shroud radius ([0.081 m, 0.12 m]), calculating the parameters and find the lowest relative Mach number. The shroud radius of 0.087m with relative Mach number of 0.727 is calculated.

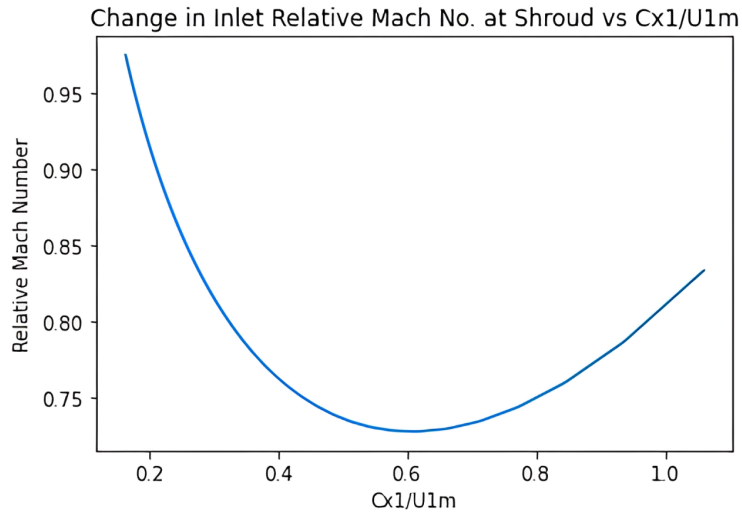


Figure 3.6: Change in inlet relative Mach number at shroud vs.  $Cx/U1m$

### 3.2.4 Inlet Incidence Angle

Inlet incidence angle should be as low as possible to minimize the incidence loss, while provides at least 1% to 2% choke margin at diffuser throat. In this project the following incidence angles for hub, mean and shroud is assumed.

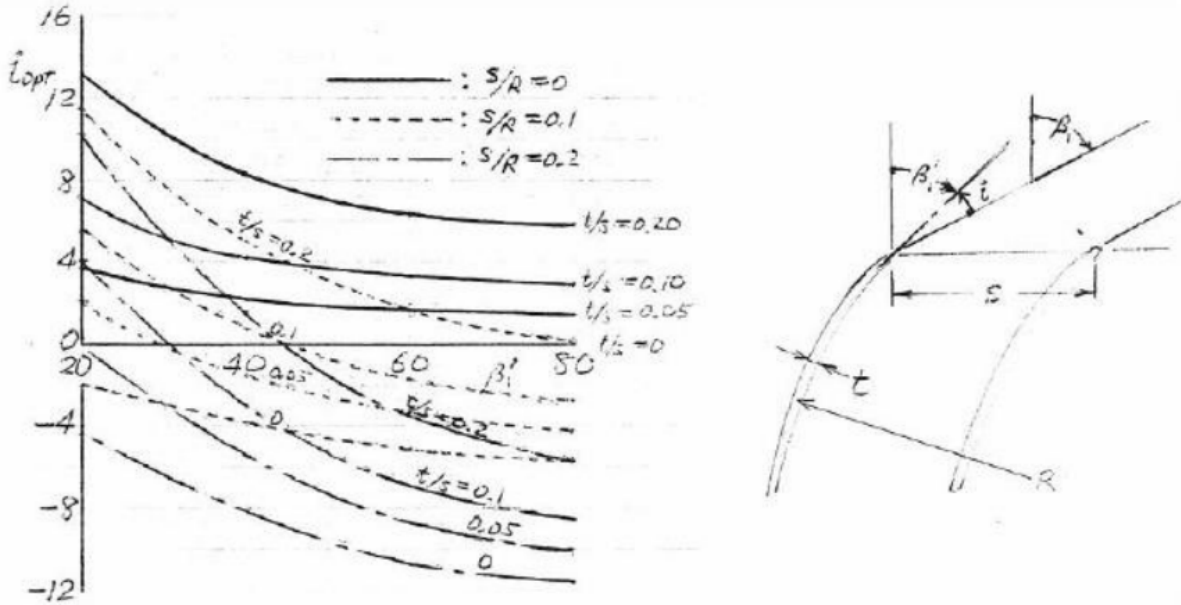


Figure 3.7: Impeller eye incidence angles vs. metal angles plots [7]

Incidence Angle	Values
$i_{1h}$	7°
$i_{1m}$	3.5°
$i_{1sh}$	2°

Table 3.3: Incidence angles at inlet of impeller

### 3.2.5 Inlet Data

Knowing the geometry of inlet design, provides us the aerodynamic parameters which help us to find the velocity triangles. As the radius at hub and shroud is defined, it is possible to find the area and axial velocity at inlet through mass conservation law.

$$A_1 = \pi \cdot (r_{1sh}^2 - r_{1h}^2) = \pi \cdot (0.087^2 - 0.06357^2) = 0.01107 \text{ m}^2$$

$$C_{x1} = \frac{\dot{m}_1}{\rho_1} \cdot A_1 = 170.602 \text{ m/s}$$

### 3.2.6 Inlet velocity Triangles

As the parameters in inlet are defined, it is possible to sketch the velocity triangles at inlet for hub, mean, and shroud. In the following table, the data related to velocity triangles are provided.

Radius	$\alpha_1$ (degree)	$\beta_1$ (degree)	$\beta_1^*$ (degree)	$C_{x1}$ (m/s)	$U_1$ (m/s)	$C_1$ (m/s)	$W_1$ (m/s)
Hub	20	45.05	38.05	170.602	233	11.55	241.48
Mean	20	51.41	47.91	170.602	275.93	181.55	273.55
Shroud	20	56.4	54.4	170.602	318.7	181.55	308.28

Table 3.4: Impeller inlet parameters at different radii

In which,  $\beta_1$  shows the relative flow angle and  $\beta_1^*$  defines the blade angle. Also, velocity triangles at hub, mean, and shroud are illustrated in the following figure :

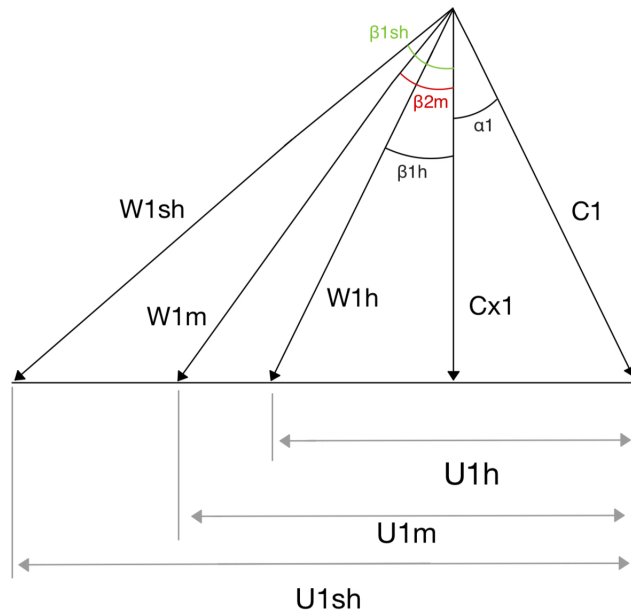


Figure 3.8: Impeller inlet velocity triangles

## 3.3 Impeller Exit Optimization

### 3.3.1 Impeller Exit Back Sweep Angle

To obtain the data for the outlet of the impeller, an exit back sweep angle ( $\beta_2^*$ ) should be selected and based on the inlet flow angle ( $\alpha_1$ ), corrected rotational velocity at exit can be calculated. In

the charts below for pressure ratio equal to 3 and the range for exit back sweep angle, corrected exit rotational velocity is calculated. Then, based on the formula for corrected velocity, real rotational velocity is calculated.

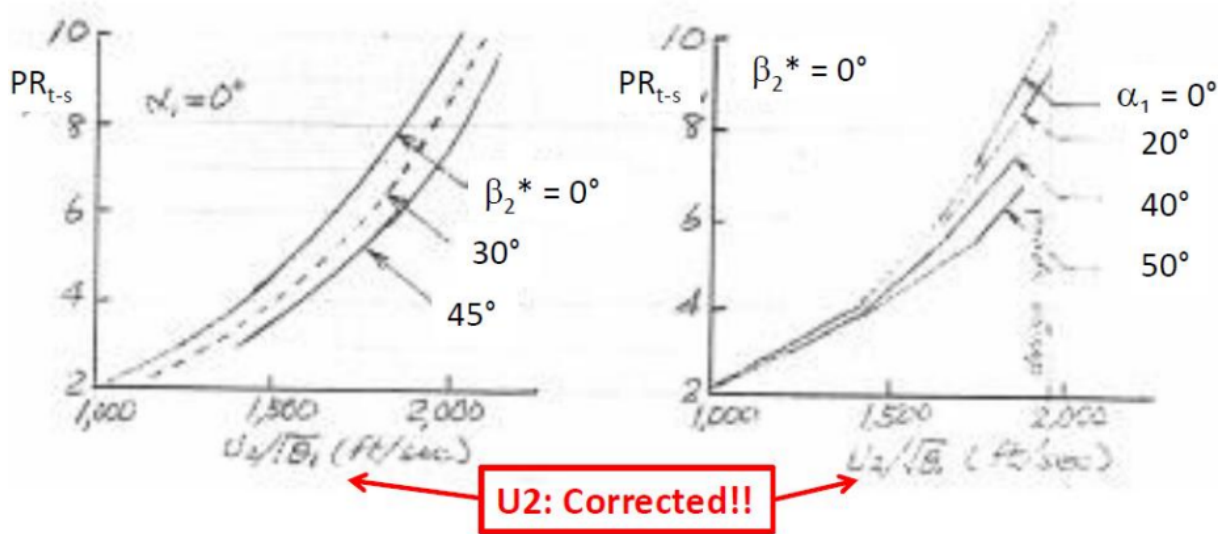


Figure 3.9: Pressure ratio vs. corrected tip tangential velocity ( $U_2$ ) at  $\alpha$  and  $\alpha_r = 0$  [7]

$$U_{2\_corrected} = \frac{U_2}{\sqrt{\theta_1}}$$

In which,

$$\theta_1 = \frac{T_{02}}{518.7^\circ R}$$

Having  $U_2$  at exit and rotational speed ( $N$ ), it is possible to find the exit radius ( $r_2$ ).

$$r_2 = \frac{U_2}{N} = 0.139 \text{ m}$$

Tangential absolute velocity at exit ( $C_{\theta 2}$ ) can be obtained from the Euler equation as follows :

$$\Delta h_0 = U_2 \cdot C_{\theta 2} - U_1 \cdot C_{\theta 1}$$

$$C_{\theta 2\infty} = \frac{(\Delta h_0 + U_1 \cdot C_{\theta 1})}{U_2}$$

Afterwards, relative hypothetical tangential velocity ( $W_{\theta 2\infty}$ ) is calculated from velocity triangles.

$$W_{\theta 2\infty} = U_2 - C_{\theta 2\infty}$$

Then, real relative flow angle ( $\beta_2$ ) is assumed in such a way that is greater than  $\beta_2^*$  in absolute value (Note:  $\beta$  at exit is negative). By knowing the relative hypothetical tangential velocity ( $W_{\theta 2\infty}$ ) and using assumed  $\beta_2$ , axial velocity at exit  $C_{r 2}$  (which is assumed to be constant in real and hypothetical, since the mass flow rate is conserved) is calculated.

$$C_{r2} = \frac{W_{\theta 2}}{\tan(\beta_2)}$$

The real relative velocity ( $W_2$ ) is calculated using the real  $\beta_2$ .

$$W_2 = \frac{W_{\theta 2}}{\sin(\beta_2)}$$

Graphs for relative velocity distribution depict that the ratio between  $W_2/W_{1sh}$  needs to be in a range between 0.5 (aggressive design) up to 0.6 (conservative design).

Furthermore, meridional velocity ratio ( $C_{r2}/C_{x1}$ ) between 0.8 to 1.0 is acceptable for the project design. Using the specified ranges, the relative velocity distribution and meridional velocity ratio is assessed. The iterative process for increment of  $\beta_2$  is continued to get the desired results based on our criteria.

Another iterative process needs to be done to find a suitable  $\beta_2^*$  which satisfy the aerodynamic slip factor. Aerodynamic slip factor is defined as the ratio between real tangential absolute velocity ( $C_{\theta 2}$ ) and hypothetic tangential absolute velocity ( $C_{\theta 2\infty}$ ). According to Stanitz's equation, aerodynamic slip factor is equal to :

$$\sigma = 1 - \left( \frac{0.63\pi}{N_b} \right)$$

in which  $N_b$  is the number of blades at impeller exit (32).

Using equation for hypothetical relative tangential velocity and Stanitz's equation, it is possible to find  $C_{\theta 2\infty}$  and  $\beta_2^*$  (it is assumed that  $C_{r2}$  is constant due to mass conservation). Comparing the new  $\beta_2^*$  with the assumed  $\beta_2^*$ , if the difference is small, the assumed  $\beta_2^*$  can be used for further calculations. The iterative process for  $\beta_2^*$  is done for the range [-40°, 0°] and increment of  $\beta_2$  is started from zero to 30 degrees with a step size of 0.2 degrees. The calculated data is tabulated below:

Variable	Amount
$r_2$	0.1397 m
$\beta_2^*$	-19.5°
$U_2$	512.14 m/s
$\beta_2$	-27.99°
$W_2/W_{1sh}$	0.599
$C_{r2}/C_{1x}$	0.956
$C_{r2}$	163.137 m/s
$C_{\theta 2}$	425.4 m/s

Table 3.5: Variables and amounts

### 3.3.2 Exit Aerodynamic and Thermodynamics Condition at Blade Exit

In this step, by using the real relative flow angle ( $\beta_2$ ) the velocity triangle is completed.

Variable	Amount
$C_2$	455.61 m/s
$\alpha_2$	69.018°
$W_2$	184.76 m/s
$\beta_2$	-27.99°

Table 3.6: Parameters at blade exit

The velocity triangle at blade exit is sketched below :

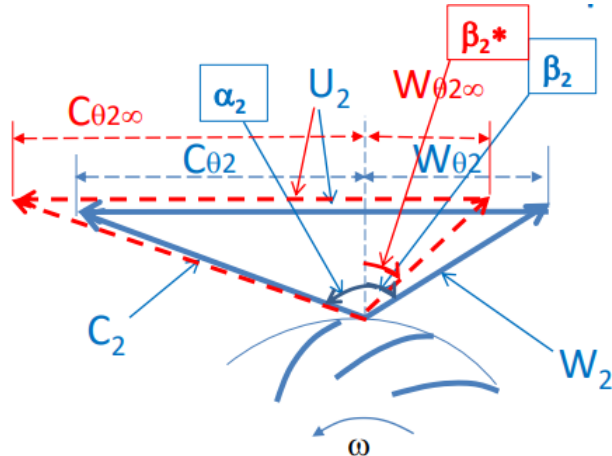


Figure 3.10: Impeller blade exit velocity triangles [7]

Thanks to the following graph, one can check if impeller tip absolute velocity ( $C_2$ ) is in stable region. Due to aerodynamic reasons, excesses  $B_2$  needed to be avoided. Thus, the graph below was created with the collective knowledge of years of research and used a guide to make sure that impeller tip absolute velocity ( $C_2$ ) is stable.

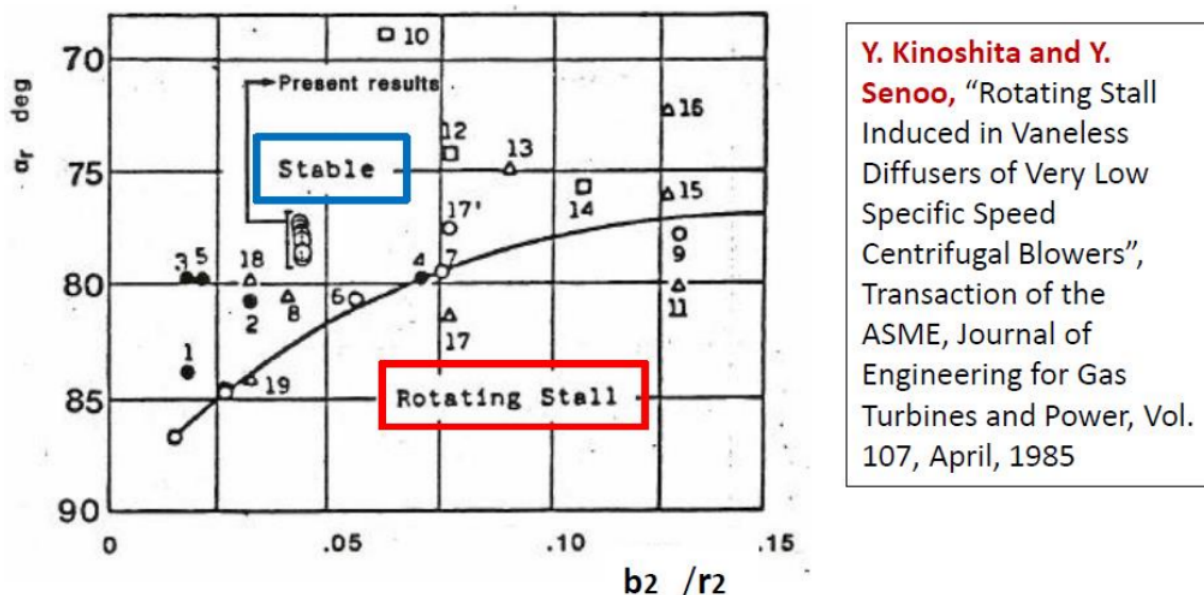


Figure 3.11: Graph for check for tip absolute velocity stability [7]

### 3.3.3 Impeller Exit Channel Height and Axial Tip Clearance

To find the blade exit channel height, the following formula is used :

$$b_2 = \frac{\dot{m}}{2\pi \cdot \rho_2 \cdot r_2 \cdot C_{r2} \cdot (1 - B_2^*)} = 0.01085 \text{ m}$$

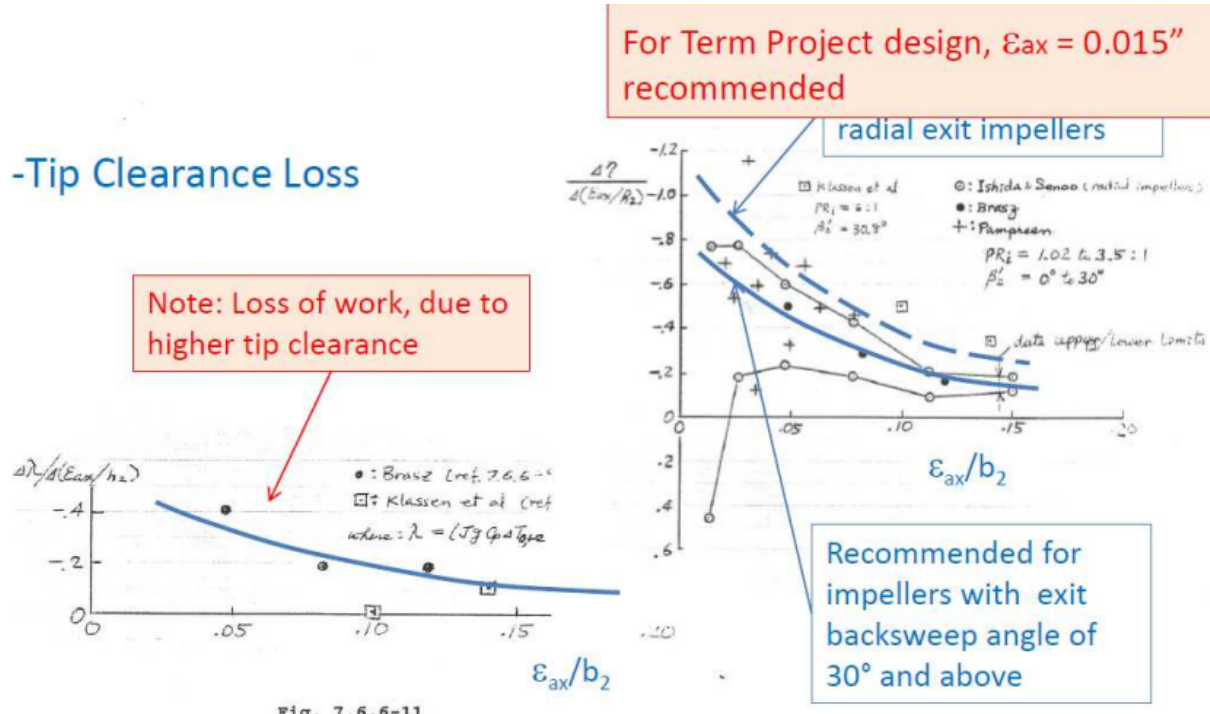


Figure 3.12: Work loss due to change in tip clearance plots [7]

$B_2$  is the blockage constant and is assumed to be 0.19. The other parameters are obtained from the previous section and are tabulated below.

Variable	Amount
$M_{2\_abs}$	0.96
$P_{02}$	1203.879 kPa
$\rho_2$	4.14 kg/m <sup>3</sup>
$M_{2\_rel}$	0.389
$r_2$	0.1397 m
$C_{r2}$	163.137 m/s

Table 3.7: Values of the different parameters calculated

Axial tip clearance for the project is recommended to be equal to 0.015 m.

### 3.3.4 Impeller Axial Length

Impeller axial length is a function of loading (pressure ratio) and inlet hub radius and recommended range for that is as below :

$$0.9 \leq \frac{(r_2 - r_{1h})}{L} \leq 1.2$$

A recommended range is  $0.9 \leq \frac{r_2 - r_{1h}}{L} \leq 1.2$

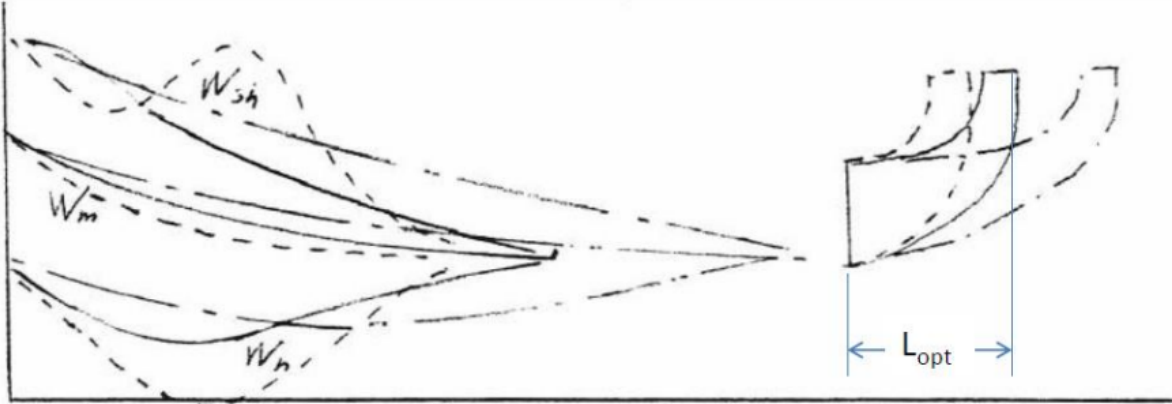


Figure 3.13: Impeller span to axial length ratio visualisation [7]

The ratio is assumed to be 1.05 and the corresponding impeller axial length is 0.06923 m.

### 3.4 Vaneless Space Geometry and Diffuser Exit Design

The absolute tangential velocity at the vaned diffuser inlet (point 3) of a centrifugal compressor can be determined by means of an angular momentum analysis.

$$C_{\theta 3} = C_{\theta 2} \times \left( \frac{r_2^2}{r_3} \right)$$

Also, through mass conservation law, it is possible to find  $C_{r3}$ .

$$C_{r3} = C_{r2} \times \left( \frac{r_2 \cdot \rho_2 \cdot (1 - B_2)}{r_3 \cdot \rho_{03} \cdot (1 - B_3)} \right)$$

In which, total density (calculated from the ideal gas law) is used instead of static density for the first guess and blockage ( $B_3$ ) is assumed to be 0.04. Afterwards, by tangential and radial components of absolute velocity,  $C_3$  and absolute Mach number are calculated. Later, an iterative process is implemented to find the static density. This is done by using the relation for total to static density, finding the new absolute velocity and trying to minimize the error between the old and new values.

$$\left( \frac{\rho_0}{\rho} \right) = \left( 1 + \frac{\gamma - 1}{2} \cdot M^2 \right)^{\frac{1}{\gamma-1}}$$

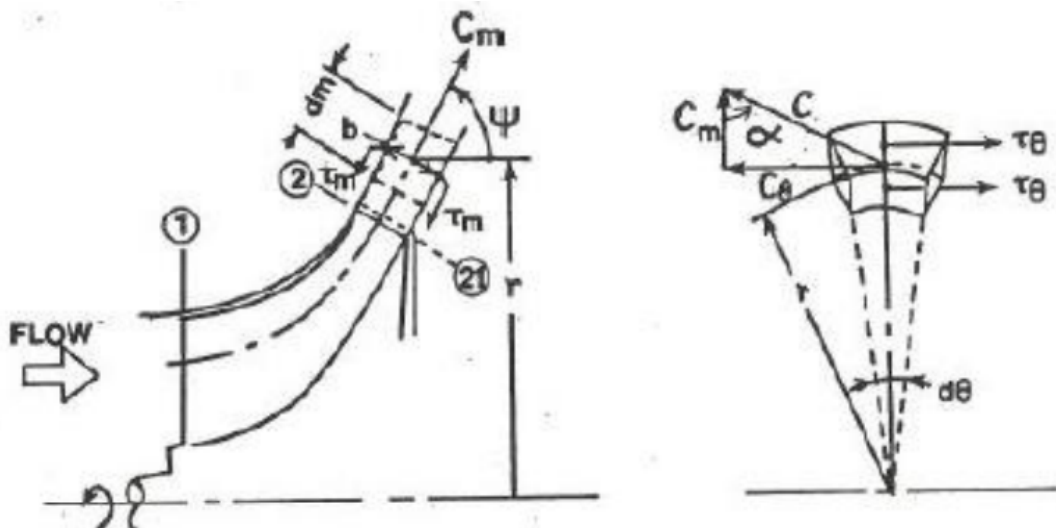


Figure 3.14: First diffuser leading edge velocity triangle [7]

The data that is obtained from the process is provided in the following table :

Variable	Amount
$C_{\theta 3}$	395.722 m/s
$C_{r3}$	119.343 m/s
$\rho_{03}$	6.265 kg/m <sup>3</sup>
$\rho_3$	4.445 kg/m <sup>3</sup>
$C_3$	413.326 m/s
$\alpha_3$	73.21°
$M_3$	0.857
$P_3$	737.05 kPa

Table 3.8: Values of the different parameters calculated

The diffuser throat is optimized to handle both choked and un-choked conditions by adjusting its area, the number of vanes, and the incidence angle simultaneously. This optimization ensures that the aspect ratio and choke margin conditions are maintained.

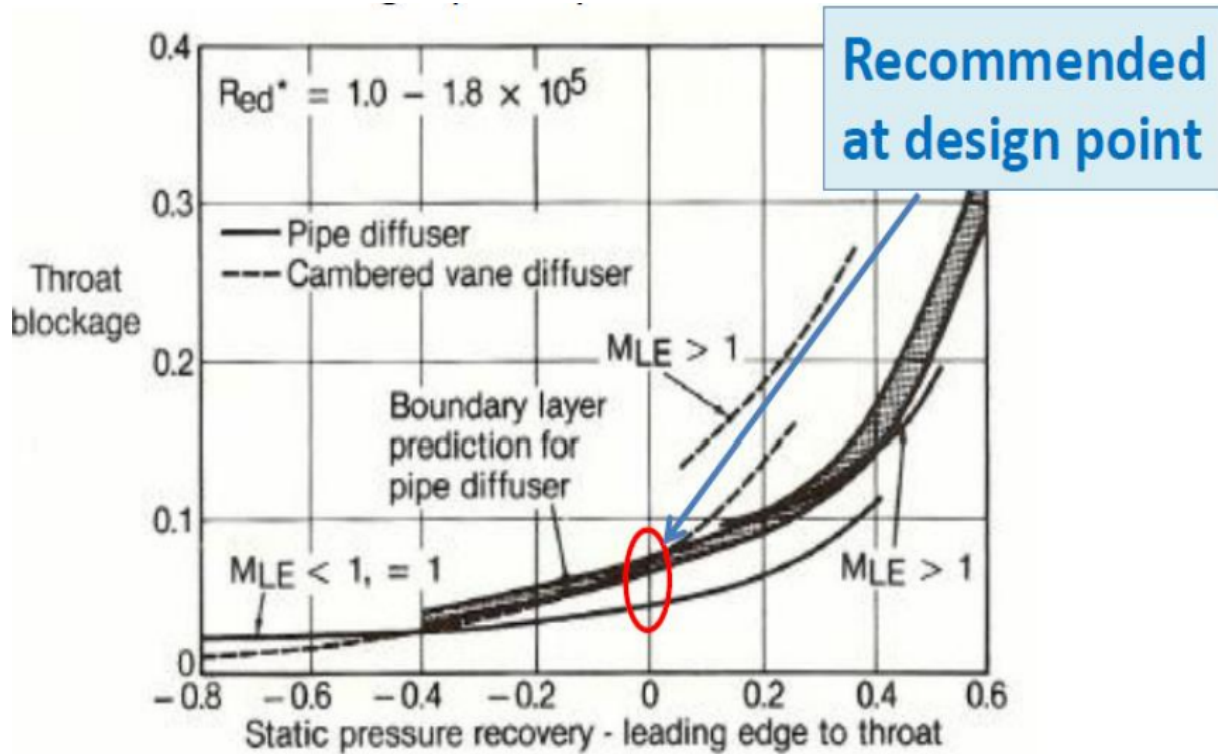


Figure 3.15: Static pressure recovery variation with block graph [7]

To find the parameters in the diffuser throat, the pressure at throat is assumed equal to static pressure at the leading edge ( $P_3$ ). Furthermore, the throat blockage  $B_3^*$  is assumed to be 0.04, between the range of 0.03 to 0.05. The flow incidence angle at the diffuser leading edge is obtained from the following chart. For the throat blockage of 0.04, the incidence angle is equal to  $-4.7^\circ$ . Then, the diffuser inlet vane angle is calculated as :

$$\alpha_3^* = \alpha_3 - i_3$$

The number of vanes ( $N_v$ ) is calculated from an iterative process in which the mass flow rate with a choke margin of 1.25% is calculated. The diffuser is designed to choke at a little bit higher mass flow than the design mass flow at the design speed, to ensure that compressor performance is high at the design point.

$$m^* = 1.0125 \times \dot{m}$$

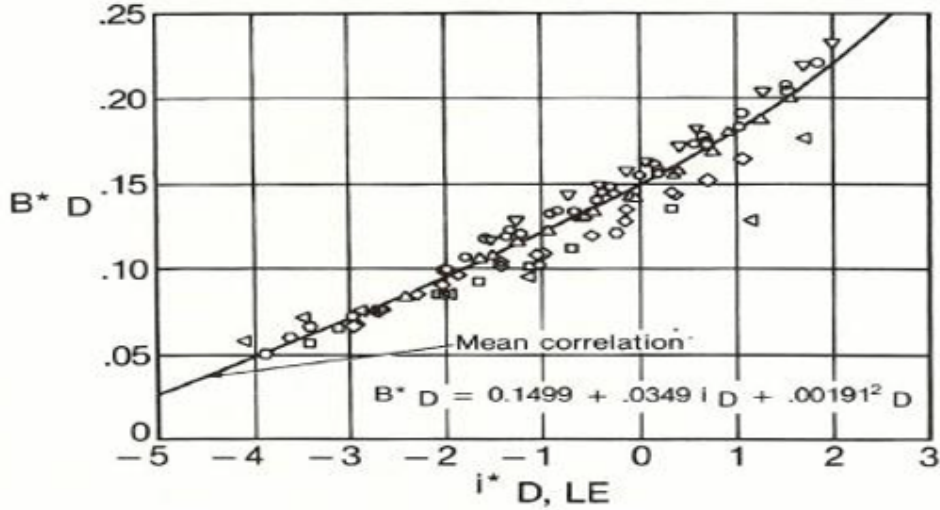


Figure 3.16: Vanned throat incidence angle variation with block [7]

Then, the throat area is calculated using the equations at the throat, knowing that  $M^*$  is the throat Mach number,  $T_0^*$  and  $P_0^*$  are equal to  $T_{03}$  and  $P_{03}$  respectively. Afterwards, the area is divided by the number of assumed vanes to find each individual throat area and throat width ( $w^*$ ). Individual throat area are calculated as follows :

$$a^* = \frac{A^*}{Nv} = b^* \times w^*$$

Furthermore, by assuming the same channel height as vaneless diffuser ( $b^* = b_3$ ), it is possible to find the throat aspect ratio. This ratio needs to be less than 1.2 and greater than 0.8.

$$\text{Throat Aspect Ratio (TAR)} = \frac{b^*}{w^*}$$

If the assumed number of vanes does not satisfy the range for throat aspect ratio, the number of vanes will increase until convergence. The following table contains the data derived from the process :

Variable	Amount
$i_3$	-4.7°
$\alpha_3^*$	77.517°
$m^*$	5.281 kg/s
$T_0^*$	662.78 K
$P_0^*$	1191.840 kPa
$A^*$	0.00294 m <sup>2</sup>
$a^*$	$15.47 \times 10^{-5}$ m <sup>2</sup>
$b^*$	0.01085 m
$w^*$	0.01354 m
TAR	0.8011
$N_v$	20
$P^*$	737.05 kPa

Table 3.9: Values of the different parameters calculated

The diffuser vane count, denoted as  $N_v$ , is intentionally kept lower than the impeller blade count,  $N_b$ , with a ratio of  $N_b/N_v = 1.6$ . This non-simple integer ratio helps prevent resonance issues in the impeller blades. The diffuser wedge angle ( $\omega$ ) refers to the angle formed by the vanes in the vaned diffuser, which determines the location of the throat. In this project, for simplicity, the vanes are assumed to have sharp leading edges, although in reality, they may not. The wedge angle can be calculated by finding the contact point between the tangency circle of the throat (Cthr) and the suction surface line of vane number 2 (line V2ss).

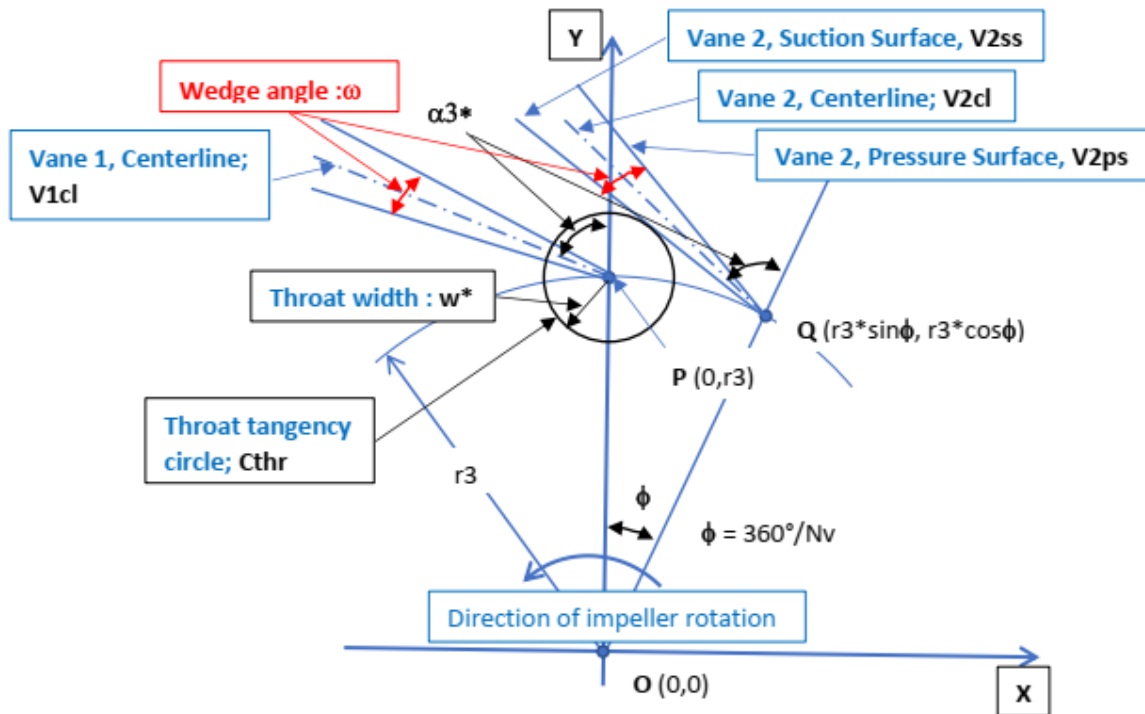


Figure 3.17: Velocity triangle for vane [7]

In order to find the Wedge angle, it is necessary to find the Diffusion angle ( $2\phi$ ). Diffusion angle is the angle between the pressure surface of vane 1 and the following vane suction surface or it can be calculated through the number of vanes.

$$\phi = \frac{360}{N_v} = 18 \text{ degrees}$$

A script is provided to find the exact wedge angle. The process is as follows :

1. Assuming an initial wedge angle.
2. Finding the distance between point  $P$  (center of circle Cthr and V2ss line).
3. If the distance is greater than the throat width ( $w^*$ ), the wedge angle is increased (No touch).
4. If the distance is lower than the throat width ( $w^*$ ), the wedge angle is decreased (touch is in two points).
5. If the distance is exactly equal to the throat width ( $w^*$ ) then the line V2ss exactly touches the circle in a single point and the wedge angle is found.

The following table summarizes the data for the wedge characteristics :

<b>Variable</b>	<b>Amount</b>
$\phi$	18°
$2\phi$	36°
$\omega$	9.45°
$\alpha_3^*$	77.517°

Table 3.10: Data for the wedge characteristics

# Chapter 4

## PART C - HPT DESIGN

### 4.1 Design Preliminary Considerations

#### 4.1.1 Given Data

Here also, the following data were given to drive the turbine design :

Parameter Name	Value
Inlet Mach number	0.125
Inlet Swirl	10° (relative to axial)
Exit Mach number	0.3 - 0.55
Exit Swirl	10° - 40° (relative to axial)
Target field life	5000 hours

Table 4.1: Stage given data

Parameter Name	Value
Aspect Ratio	0.5
Zweifel Coefficient at Mean	0.75 - 0.90
Trailing Edge Thickness (minimum)	0.05 in

Table 4.2: Vane given data

Parameter Name	Value
Aspect Ratio	1.3
Zweifel Coefficient at Mean	0.8 - 0.95
Trailing Edge Thickness (minimum)	0.03 in
Tip Clearance to Span	1 - 2%

Table 4.3: Blade given data

Parameter Name	Value
$AN^2$	$\leq 3.5 \times 10^{10}$
Rim Speed	1100 ft/s

Table 4.4: Blade Containment Consideration

#### 4.1.2 HPT Design Assumptions

- Steady State and Steady Flow
- Adiabatic control volume
- Free Vortex theory for hub and tip calculations
- Constant hub radius
- Constant RPM at the design point, so constant angular velocity
- For vane loss calculations average tip radius is utilized
- $0^\circ$  incidence and deviation angle at design condition
- Converging flow path for the vane ( $A_1 > A_2$ ) and a constant cylindrical section ( $A_2 = A_3$ ) for the blade is considered

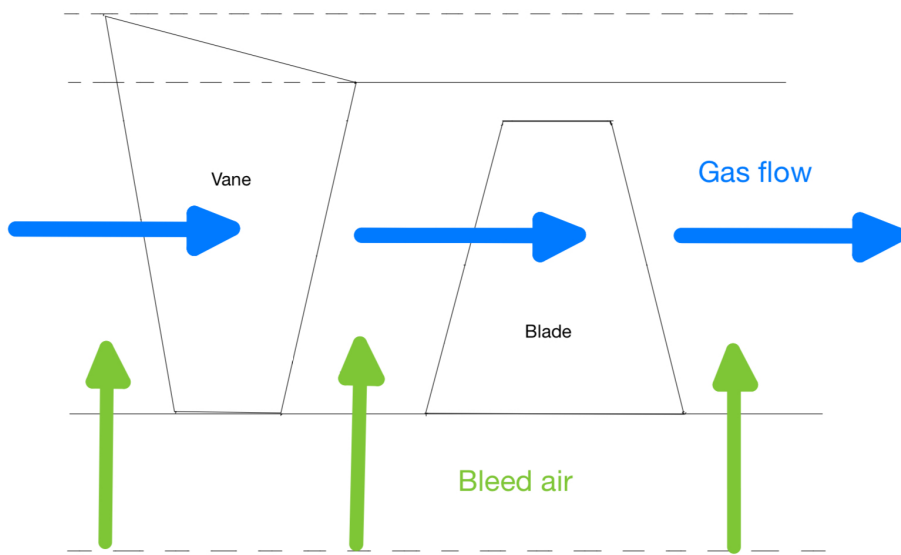


Figure 4.1: Axial gas flow

#### 4.1.3 Blade Containment Considerations

- $P_{01} > P_{02} > P_{03}$  and  $P_{02r} > P_{03r}$  across the stage
- $A_1 > A_2 = A_3$
- Vane trailing edge thickness  $t_{te,v} \geq 0.00127\text{ m}$
- Blade trailing edge thickness  $t_{te,b} \geq 0.000762\text{ m}$
- Reaction for the whole span of the blade should always be positive

#### 4.1.4 Constraints

To stay within the structural limits of the blade induced by the rotation of the blade. Few limits on rotational speed are considered :

- $AN^2 \leq 3.5 \times 10^{10} \text{ inch}^2 \text{ RPM}^2$
- Rim speed  $U_h \leq 335.28\text{ m/s}$

#### 4.1.5 Radius Relations for Hub, Mean and Tip Sections

$$A = \pi(r_t^2 - r_h^2)$$

$$r_m = \frac{1}{2}(r_t + r_h)$$

$$r_t = r_m + \frac{A}{4\pi r_m}$$

### 4.2 Design methodology

#### 4.2.1 Velocity triangles

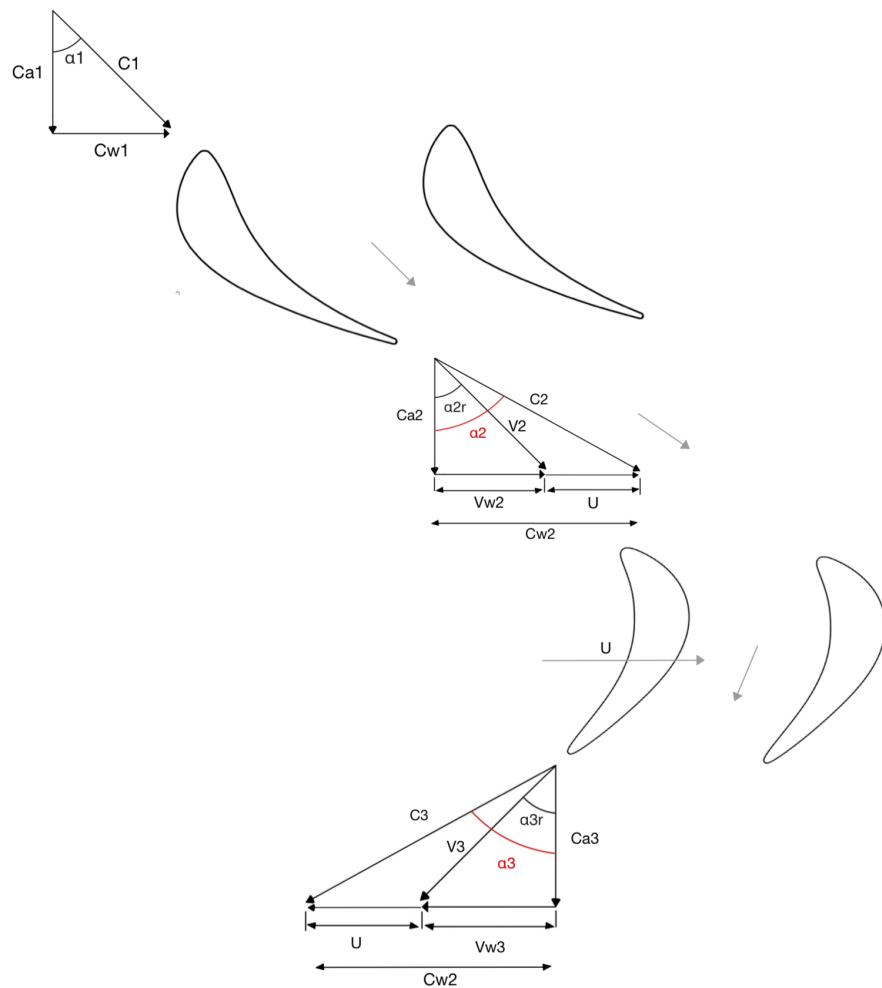


Figure 4.2: Turbine velocity triangles

#### 4.2.2 Step - 1

Defining mass flow rate, static temperature and static pressure at the exit of the vane i.e. location - 1. Also, determine static density and effective area from mass flow rate and absolute velocity component. These elementary properties are used to define the inlet velocity triangle of the vane profile.

$$\dot{m}_1 = \dot{m}_a (1 - \beta_{HPC}) + \dot{m}_f$$

$$T_1 = \frac{T_{01}}{\left(1 + \frac{\gamma_g - 1}{2} M_{1m}^2\right)}$$

$$P_1 = \frac{P_{01}}{\left(1 + \frac{\gamma_g - 1}{2} M_{1m}^2\right)^{\frac{\gamma_g}{\gamma_g - 1}}}$$

$$C_{1m} = M_{1m} \sqrt{\gamma_g R_g T_1}$$

$$C_{a1m} = C_{1m} \cos \alpha_{1m}$$

$$C_{w1m} = C_{a1m} \tan \alpha_{1m}$$

$$\rho_1 = \frac{P_1}{R_g T_1}$$

$$A_{1m} = \frac{\dot{m}_1}{\rho_1 C_{a1m}}$$

#### 4.2.3 Step - 2

Define mass flow rate, static temperature and static pressure at the exit of the blade i.e. location - 3. Also, determine static density and effective area from mass flow rate and absolute velocity component.

$$\dot{m}_3 = \dot{m}_a (1 - \beta_{HPC} + \beta_{S,HPT} + \beta_{D,HPT})$$

$$T_3 = \frac{T_{03}}{\left(1 + \frac{\gamma_g - 1}{2} M_{3m}^2\right)}$$

$$P_3 = \frac{P_{03}}{\left(1 + \frac{\gamma_g - 1}{2} M_{3m}^2\right)^{\frac{\gamma_g}{\gamma_g - 1}}}$$

$$C_{3m} = M_{3m} \sqrt{\gamma_g R_g T_3}$$

$$C_{a3m} = C_{3m} \cos \alpha_{3m}$$

$$C_{w3m} = C_{a3m} \tan \alpha_{3m}$$

$$\rho_3 = \frac{P_3}{R_g T_3}$$

$$A_{3m} = \frac{\dot{m}_3}{\rho_3 C_{a3m}}$$

#### 4.2.4 Step - 3

Define mass flow rate, static temperature, and static pressure at the entry of the blade i.e. location - 2. Also, determine static density and effective area from mass flow rate and absolute velocity component. To find the static temperature at location - 2, consider temperature based reaction and find temperature based on the assumed value of reaction at the mean.

$$\dot{m}_2 = \dot{m}_a (1 - \beta_{HPC} + \beta_{S,HPT}) + \dot{m}_f$$

$$T_2 = R_m (T_1 - T_3) + T_3$$

$$P_2 = P_{02} \left( \frac{T_2}{T_{02}} \right)^{\frac{\gamma_g}{\gamma_g - 1}}$$

$$C_{2m} = \sqrt{2Cp_g(T_{02} - T_2)}$$

$$\rho_2 = \frac{P_2}{R_g T_2}$$

$$C_{a2m} = \frac{\dot{m}_2}{\rho_2 A_{2m}}$$

$$C_{w2m} = \sqrt{C_{2m}^2 - C_{a2m}^2}$$

$$\tan \alpha_{2m} = \frac{C_{w2m}}{C_{a2m}}$$

$$M_{2m} = \frac{C_{2m}}{\sqrt{\gamma_g R_g T_2}}$$

#### 4.2.5 Step - 4

From Step 2 and Step 3, we have geometrical parameters for velocity triangles. Although we need to construct an entire blade profile, for that we need  $r_{t,b}$  and  $r_{h,b}$ . For this, consider Euler's work equation to find  $U_m$ .

From  $U_m$ , we have considered  $r_{t,b}$  and  $r_{h,b}$ .

$$U_m = \frac{\dot{W}_{HPT}}{\dot{m}_2 C_{w2m} - \dot{m}_3 C_{w3m}}$$

$$r_{m,b} = \frac{60U_m}{2\pi N}$$

$$\omega = \frac{U_m}{r_{m,b}}$$

$$r_{t,b} = r_{m,b} + \frac{A_{3m}}{4\pi r_{m,b}}$$

$$r_{h,b} = 2r_{m,b} - r_{t,b}$$

Tip clearance is taken as constant  $\Delta t_c = 2\%$  of blade span. From that total height of the blade is governed using the following equation.

$$h_b = 0.98(r_{t,b} - r_{h,b})$$

$$r_{h,v} = r_{h,b}$$

$$r_{t,v,in} = \sqrt{\frac{A_{1m}}{\pi} + r_{h,v}^2}$$

$$r_{t,v,out} = r_{t,b}$$

$$r_{t,v,avg} = \frac{r_{t,v,in} + r_{t,v,out}}{2}$$

$$r_{m,v} = \frac{r_{t,v,avg} + r_{h,v}}{2}$$

$$h_v = (r_{t,v,avg} - r_{h,v})$$

#### 4.2.6 Step - 5

Although we have absolute velocities and angles for the velocity triangle, we have to find the relative parameters of velocity triangles at the entry of the blade i.e. location - 2.

$$V_{w2m} = C_{w2m} - U_m$$

$$V_{2m} = \sqrt{C_{a2m}^2 + V_{w2m}^2}$$

$$\tan\alpha_{2rm} = \frac{V_{w2m}}{C_{a2m}}$$

$$M_{2r} = \frac{V_{2m}}{\sqrt{\gamma_g R_g T_2}}$$

$$T_{02r} = T_2 + \frac{V_{2m}^2}{2Cp_g}$$

$$P_{02r} = P_2 \left( \frac{T_{02r}}{T_2} \right)^{\frac{\gamma_g}{\gamma_g - 1}}$$

#### 4.2.7 Step - 6

Also, repeating the same procedure at the exit of the blade i.e. location - 3 to find relative parameters.

$$V_{w3m} = C_{w3m} + U_m$$

$$V_{3m} = \sqrt{C_{a3m}^2 + V_{w3m}^2}$$

$$\tan\alpha_{3rm} = \frac{V_{w3m}}{C_{a3m}}$$

$$M_{3r} = \frac{V_{3m}}{\sqrt{\gamma_g R_g T_3}}$$

$$T_{03r} = T_3 + \frac{V_{3m}^2}{2Cp_g}$$

$$P_{03r} = P_3 \left( \frac{T_{03r}}{T_3} \right)^{\frac{\gamma_g}{\gamma_g - 1}}$$

#### 4.2.8 Results from Off Design Analysis:

The results shown below are from the design point speed, which is  $N = 35,000 \text{ RPM}$

Parameter Name	Symbol	Value
Mach Number - 1	$M_1$	0.1250
Absolute Velocity - 1	$C_1$	86.394 m/s
Axial Velocity - 1	$C_{a1}$	85.082 m/s
Tangential Velocity - 1	$C_{w1}$	-15.002 m/s
Absolute Flow Angle - 1	$\alpha_1$	-10.000°
Static Temperature - 1	$T_1$	1248.642 K
Static Pressure - 1	$P_1$	1169.784 kPa
Total Temperature - 1	$T_{01}$	1251.890 K
Total Pressure - 1	$P_{01}$	1182.014 kPa
Mach Number - 2	$M_2$	0.7929
Absolute Velocity - 2	$C_2$	518.017 m/s
Axial Velocity - 2	$C_{a2}$	180.185 m/s
Tangential Velocity - 2	$C_{w2}$	485.669 m/s
Absolute Flow Angle - 2	$\alpha_2$	69.645°
Static Temperature - 2	$T_2$	1115.457 K
Static Pressure - 2	$P_2$	793.223 kPa
Total Temperature - 2	$T_{02}$	1231.330 K
Total Pressure - 2	$P_{02}$	1182.014 kPa
Mach Number - 3	$M_3$	0.5250
Absolute Velocity - 3	$C_3$	323.905 m/s
Axial Velocity - 3	$C_{a3}$	293.557 m/s
Tangential Velocity - 3	$C_{w3}$	136.888 m/s
Absolute Flow Angle - 3	$\alpha_3$	25.000°
Static Temperature - 3	$T_3$	994.956 K
Static Pressure - 3	$P_3$	447.305 kPa
Total Temperature - 3	$T_{03}$	1040.616 K
Total Pressure - 3	$P_{03}$	535.315 kPa

Table 4.5: Mean line absolute results

Parameter Name	Symbol	Value
Relative Mach Number - 2	$M_{2r}$	0.3505
Relative Velocity - 2	$V_2$	228.997 m/s
Relative Tangential Velocity - 2	$V_{w2}$	141.326 m/s
Relative Flow Angle - 2	$\alpha_{2r}$	38.108°
Total Relative Temperature - 2	$T_{02r}$	1138.296 K
Total Relative Pressure - 2	$P_{02r}$	860.213 kPa
Relative Mach Number - 3	$M_{3r}$	0.9137
Relative Velocity - 3	$V_3$	563.701 m/s
Relative Tangential Velocity - 3	$V_{w3}$	481.231 m/s
Relative Flow Angle - 3	$\alpha_{3r}$	58.616°
Total Relative Temperature - 3	$T_{03r}$	1133.353 K
Total Relative Pressure - 3	$P_{03r}$	753.113 kPa

Table 4.6: Mean line relative results

#### 4.2.9 Free vortex analysis

Free vortex theory is a key concept in the design of gas turbine engines. The main principles are:

- The free vortex approach assumes that the flow through an axial gas turbine stage follows a free vortex pattern, where the circumferential velocity (tangential velocity) varies inversely with the radius [2].
- This means the product of the circumferential velocity and radius is constant.
- This free vortex flow pattern allows for the calculation of the efficiency or loss of nozzle guide vane annular cascades from experimental measurements of the downstream flow [4].
- By mixing out the measured flow to a free vortex state, a unique, lossless, isentropic reference flow can be determined. The actual efficiency is then calculated as the ratio of the experimental kinetic energy flux to this ideal isentropic kinetic energy flux.
- The free vortex theory has been used to design vortex blading, where the blade shape is tailored to match the changing gas flow angles through the turbine stage [4]. This helps to improve the aerodynamic performance compared to conventional blade designs.
- Vortex theory has been outlined in section [6] where it was shown that if the elements of fluid are to be in radial equilibrium, an increase in static pressure from root to tip is necessary whenever there is a whirl component of velocity. The proportion of the stage pressure or temperature drop that occurs in the rotor must increase from root to tip [6].

#### 4.2.10 Assumptions for free vortex design

- The stagnation enthalpy  $h_o$  is constant over the annulus (i.e.  $dh_o/dr = 0$ )
- The axial velocity is constant over the annulus
- The whirl velocity is inversely proportional to the radius

#### 4.2.11 Step - 7 : Hub and Tip absolute values

$$C_{w1h} = C_{w1m} \frac{r_{m,v}}{r_{h,v}}$$

$$C_{w1t} = C_{w1m} \frac{r_{m,v}}{r_{t,v,avg}}$$

$$C_{w2h} = C_{w2m} \frac{r_{m,b}}{r_{h,b}}$$

$$C_{w2t} = C_{w2m} \frac{r_{m,b}}{r_{t,b}}$$

$$C_{w3h} = C_{w3m} \frac{r_{m,b}}{r_{h,b}}$$

$$C_{w3t} = C_{w3m} \frac{r_{m,b}}{r_{t,b}}$$

$$\tan\alpha_{1h} = \frac{C_{w1h}}{Ca1}$$

$$\tan\alpha_{1t} = \frac{C_{w1t}}{Ca1}$$

$$\tan\alpha_{2h} = \frac{C_{w2h}}{Ca2}$$

$$\tan\alpha_{2t} = \frac{C_{w2t}}{Ca2}$$

$$\tan\alpha_{3h} = \frac{C_{w3h}}{Ca3}$$

$$\tan\alpha_{3t} = \frac{C_{w3t}}{Ca3}$$

$$C_{1h} = \frac{C_{a1}}{\tan\alpha_{1h}}$$

$$C_{1t} = \frac{C_{a1}}{\tan\alpha_{1t}}$$

$$C_{2h} = \frac{C_{a2}}{\tan\alpha_{2h}}$$

$$C_{2t} = \frac{C_{a2}}{\tan\alpha_{2t}}$$

$$C_{3h} = \frac{C_{a3}}{\tan\alpha_{3h}}$$

$$C_{3t} = \frac{C_{a3}}{\tan\alpha_{3t}}$$

$$T_{1h} = T_{01} - \frac{C_{1h}^2}{2Cp_g}$$

$$T_{1t} = T_{01} - \frac{C_{1t}^2}{2Cp_g}$$

$$T_{2h} = T_{02} - \frac{C_{2h}^2}{2Cp_g}$$

$$T_{2t} = T_{02} - \frac{C_{2t}^2}{2Cp_g}$$

$$T_{3h} = T_{03} - \frac{C_{3h}^2}{2Cp_g}$$

$$T_{3t} = T_{03} - \frac{C_{3t}^2}{2Cp_g}$$

$$M_{1h} = \frac{C_{1h}}{\sqrt{\gamma_g R_g T_{1h}}}$$

$$M_{1t} = \frac{C_{1t}}{\sqrt{\gamma_g R_g T_{1t}}}$$

$$M_{2h} = \frac{C_{2h}}{\sqrt{\gamma_g R_g T_{2h}}}$$

$$M_{2t} = \frac{C_{2t}}{\sqrt{\gamma_g R_g T_{2t}}}$$

$$M_{3h} = \frac{C_{3h}}{\sqrt{\gamma_g R_g T_{3h}}}$$

$$M_{3t} = \frac{C_{3t}}{\sqrt{\gamma_g R_g T_{3t}}}$$

$$P_{1h} = \frac{P_{01}}{\left(1 + \frac{\gamma_g - 1}{2} M_{1h}^2\right)^{\frac{\gamma_g}{\gamma_g - 1}}}$$

$$P_{1t} = \frac{P_{01}}{\left(1 + \frac{\gamma_g - 1}{2} M_{1t}^2\right)^{\frac{\gamma_g}{\gamma_g - 1}}}$$

$$P_{2h} = \frac{P_{02}}{\left(1 + \frac{\gamma_g - 1}{2} M_{2h}^2\right)^{\frac{\gamma_g}{\gamma_g - 1}}}$$

$$P_{2t} = \frac{P_{02}}{\left(1 + \frac{\gamma_g - 1}{2} M_{2t}^2\right)^{\frac{\gamma_g}{\gamma_g - 1}}}$$

$$P_{3h} = \frac{P_{03}}{\left(1 + \frac{\gamma_g - 1}{2} M_{3h}^2\right)^{\frac{\gamma_g}{\gamma_g - 1}}}$$

$$P_{3t} = \frac{P_{03}}{\left(1 + \frac{\gamma_g - 1}{2} M_{3t}^2\right)^{\frac{\gamma_g}{\gamma_g - 1}}}$$

$$U_h = \omega r_{h,b}$$

$$U_t = \omega r_{t,b}$$

$$R_h = \frac{T_{2h} - T_{3h}}{T_{1h} - T_{3h}}$$

$$R_t = \frac{T_{2t} - T_{3t}}{T_{1t} - T_{3t}}$$

#### 4.2.12 Step - 7.1 : Hub and Tip relative values

$$V_{w2h} = C_{w2h} - U_h$$

$$V_{w2t} = C_{w2t} - U_t$$

$$V_{w3h} = C_{w3h} + U_h$$

$$V_{w3t} = C_{w3t} + U_t$$

$$V_{2h} = \sqrt{V_{w2h}^2 + C_{a2}^2}$$

$$V_{2t} = \sqrt{V_{w2t}^2 + C_{a2}^2}$$

$$V_{3h} = \sqrt{V_{w3h}^2 + C_{a3}^2}$$

$$V_{3t} = \sqrt{V_{w3t}^2 + C_{a3}^2}$$

$$\tan\alpha_{2rh} = \frac{V_{w2h}}{C_{a2}}$$

$$\tan\alpha_{2rt} = \frac{V_{w2t}}{C_{a2}}$$

$$\tan\alpha_{3rh} = \frac{V_{w3h}}{C_{a3}}$$

$$\tan\alpha_{3rt} = \frac{V_{w3t}}{C_{a3}}$$

$$M_{2rh} = \frac{V_{2h}}{\sqrt{\gamma_g R_g T_{2h}}}$$

$$M_{2rt} = \frac{V_{2t}}{\sqrt{\gamma_g R_g T_{2t}}}$$

$$M_{3rh} = \frac{V_{3h}}{\sqrt{\gamma_g R_g T_{3h}}}$$

$$M_{3rt} = \frac{V_{3t}}{\sqrt{\gamma_g R_g T_{3t}}}$$

$$T_{02rh} = T_2 + \frac{V_{1h}^2}{2Cp_g}$$

$$T_{03rh} = T_3 + \frac{V_{2h}^2}{2Cp_g}$$

$$P_{02rh} = P_{02} \left( 1 + \frac{\gamma_g - 1}{2} M_{2rh}^2 \right)^{\frac{\gamma_g}{\gamma_g - 1}}$$

$$P_{03rh} = P_{03} \left( 1 + \frac{\gamma_g - 1}{2} M_{3rh}^2 \right)^{\frac{\gamma_g}{\gamma_g - 1}}$$

$$T_{02rt} = T_2 + \frac{V_{1t}^2}{2Cp_g}$$

$$T_{03rt} = T_3 + \frac{V_{2t}^2}{2Cp_g}$$

$$P_{02rt} = P_{02} \left( 1 + \frac{\gamma_g - 1}{2} M_{2rt}^2 \right)^{\frac{\gamma_g}{\gamma_g - 1}}$$

$$P_{03rt} = P_{03} \left( 1 + \frac{\gamma_g - 1}{2} M_{3rt}^2 \right)^{\frac{\gamma_g}{\gamma_g - 1}}$$

#### 4.2.13 Results from Hub and Tip Line Analysis

Parameter Name	Symbol	Hub Value	Symbol	Tip Value
Mach Number - 1	$M_{1h}$	0.1255	$M_{1t}$	0.1246
Absolute Velocity - 1	$C_{1h}$	86.771 m/s	$C_{1t}$	86.131 m/s
Axial Velocity - 1	$C_{a1h}$	85.082 m/s	$C_{a1t}$	85.082 m/s
Tangential Velocity - 1	$C_{w1h}$	-17.036 m/s	$C_{w1t}$	-13.402 m/s
Absolute Flow Angle - 2	$\alpha_{1h}$	-11.323°	$\alpha_{1t}$	-8.952°
Static Temperature - 1	$T_{1h}$	1248.611 K	$T_{1t}$	1248.659 K
Static Pressure - 1	$P_{1h}$	1169.678 kPa	$P_{1t}$	1169.858 kPa
Total Temperature - 1	$T_{01h}$	1251.890 K	$T_{01t}$	1251.890 K
Total Pressure - 1	$P_{01h}$	1182.014 kPa	$P_{01t}$	1182.014 kPa
Mach Number - 2	$M_{2h}$	0.8783	$M_{2t}$	0.7256
Absolute Velocity - 2	$C_{2h}$	567.657 m/s	$C_{2t}$	477.699 m/s
Axial Velocity - 2	$C_{a2h}$	180.185 m/s	$C_{a2t}$	180.185 m/s
Tangential Velocity - 2	$C_{w2h}$	538.301 m/s	$C_{w2t}$	442.413 m/s
Absolute Flow Angle - 2	$\alpha_{2h}$	71.493°	$\alpha_{2t}$	67.840°
Static Temperature - 2	$T_{2h}$	1091.984 K	$T_{2t}$	1132.330 K
Static Pressure - 2	$P_{2h}$	728.736 kPa	$P_{2t}$	844.384 kPa
Total Temperature - 2	$T_{02h}$	1231.330 K	$T_{02t}$	1231.330 K
Total Pressure - 2	$P_{02h}$	1182.014 kPa	$P_{02t}$	1182.014 kPa
Mach Number - 3	$M_{3h}$	0.5361	$M_{3t}$	0.5166
Absolute Velocity - 3	$C_{3h}$	330.448 m/s	$C_{3t}$	318.944 m/s
Axial Velocity - 3	$C_{a3h}$	293.557 m/s	$C_{a3t}$	293.557 m/s
Tangential Velocity - 3	$C_{w3h}$	151.722 m/s	$C_{w3t}$	124.696 m/s
Absolute Flow Angle - 3	$\alpha_{3h}$	27.332°	$\alpha_{3t}$	23.015°
Static Temperature - 3	$T_{3h}$	993.057 K	$T_{3t}$	996.311 K
Static Pressure - 3	$P_{3h}$	443.959 kPa	$P_{3t}$	449.806 kPa
Total Temperature - 3	$T_{03h}$	1040.616 K	$T_{03t}$	1040.616 K
Total Pressure - 3	$P_{03h}$	535.315 kPa	$P_{03t}$	535.315 kPa

Table 4.7: Hub and Tip absolute results

Parameter Name	Symbol	Hub Value	Symbol	Tip Value
Relative Mach Number - 2	$M_{2rh}$	0.4492	$M_{2rt}$	0.2906
Relative Velocity - 2	$V_{2h}$	290.310 m/s	$V_{2t}$	191.348 m/s
Relative Tangential Velocity - 2	$V_{w2h}$	227.626 m/s	$V_{w2t}$	64.403 m/s
Relative Flow Angle - 2	$\alpha_{2rh}$	51.635°	$\alpha_{2rt}$	19.668°
Total Relative Temperature - 2	$T_{02rh}$	1152.164 K	$T_{02rt}$	1131.404 K
Total Relative Pressure - 2	$P_{02rh}$	905.381 kPa	$P_{02rt}$	838.836 kPa
Relative Mach Number - 3	$M_{3rh}$	0.8886	$M_{3rt}$	0.9429
Relative Velocity - 3	$V_{3h}$	547.711 m/s	$V_{3t}$	582.142 m/s
Relative Tangential Velocity - 3	$V_{w3h}$	462.398 m/s	$V_{w3t}$	502.706 m/s
Relative Flow Angle - 3	$\alpha_{3rh}$	57.590°	$\alpha_{3rt}$	59.717°
Total Relative Temperature - 3	$T_{03rh}$	1125.613 K	$T_{03rt}$	1142.556 K
Total Relative Pressure - 3	$P_{03rh}$	733.398 kPa	$P_{03rt}$	777.330 kPa

Table 4.8: Hub and Tip relative results

### 4.3 Loss Model

There are different kind of losses which may occur during the performance of the turbine and determine the efficiency of the High Pressure Turbine.

Losses which we have to consider here for efficiency calculation are :

1. Profile Losses or Primary Losses
  - (a) Tip Clearance
  - (b) Trailing Edge Loss
2. Secondary losses

The method to be outlined here is due to Ainley and Mathieson, which estimates the performance on flow conditions at the mean diameter of the annulus i.e. calculate losses at design conditions. Thus, this method describes how to calculate the performance of a turbine over a range of operating conditions.

A start is made using the two correlations for profile loss coefficient  $Y_p$  obtained from cascade data, which are shown in figure: 4.8. These refer to nozzle-type blades ( $\beta_2 = 0$ ) and impulse-type blades ( $\beta_2 = \beta_3$ ) of conventional profile having a thickness/chord ratio ( $t/c$ ) of 0.2 and a trailing edge thickness/pitch ratio of 0.02.

To find out losses at design condition, we must have some geometric parameters like chord ( $C$ ), maximum thickness ( $t_c$ ), stagger angle, axial chord ( $C_a$ ) and number of blades based on Zweifel coefficient.

#### 4.3.1 Geometric Parameters

**Chord :**

Chord refers to the imaginary straight line connecting the leading edge to the trailing edge of an airfoil. In our case, chord can be determined by using the aspect ratio based on given data.

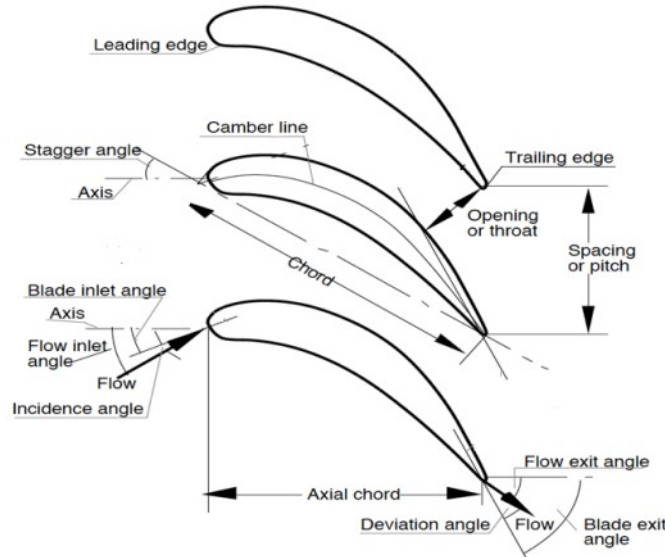


Figure 4.3: Geometrical parameters

$$C_b = \frac{h_b}{AR_b}$$

$$C_v = \frac{h_v}{AR_v}$$

#### **Maximum thickness :**

The maximum thickness of the blade profile is an important parameter in defining the aerodynamic losses of the blade. From 4.4 we can have ratio of  $\frac{t_{max}}{C}$  with the help of  $\beta_1 + \beta_2$ .

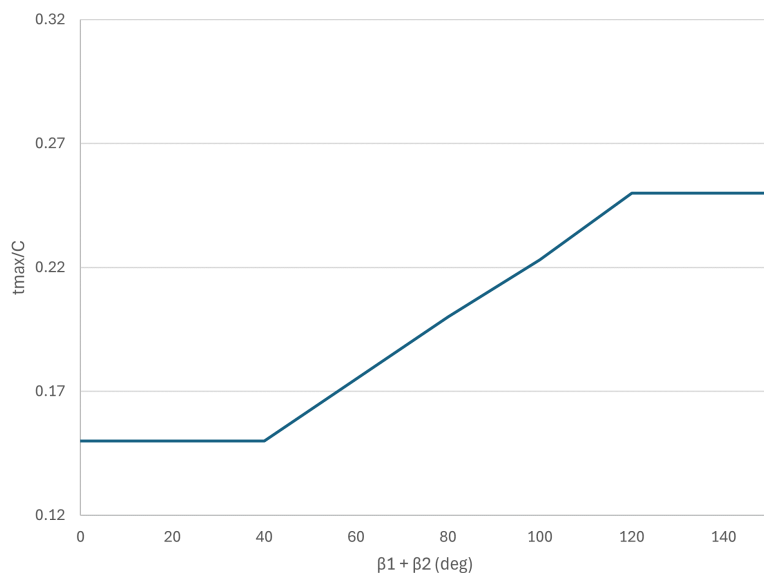


Figure 4.4:  $t_{max}/C$  vs  $\beta_1 + \beta_2$  [4]

$$t_{max,b} = \frac{t_{max}}{C} C_b$$

$$t_{max,v} = \frac{t_{max}}{C} C_v$$

**Stagger angle :**

The stagger angle refers to the angle between the chord line of the blade and the direction of the fluid flow (often referred to as the relative flow angle).

When discussing axial-flow turbines, which are commonly used in gas turbines or steam turbines, the stagger angle plays a critical role in determining the efficiency and performance of the turbine. By adjusting the stagger angle, engineers can optimize the turbine for specific operating conditions, such as varying fluid velocities and temperatures.

Stagger angle can be found from the figure: 4.5 using inlet and exit blade metal angles.

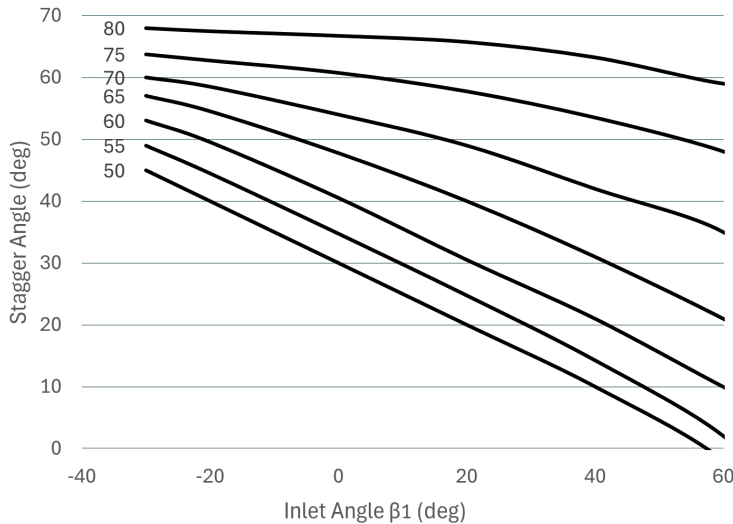


Figure 4.5: Inlet Angle vs Stagger Angle [4]

**Axial chord :**

Axial chord can be found by the cosine of the stagger angle with the actual chord.

$$C_{a,b} = C_b \cos \phi_b$$

$$C_{a,v} = C_v \cos \phi_v$$

**Pitch :**

$$s_b = \frac{\psi_b C_{a,b}}{2(\tan \alpha_{2rm} + \tan \alpha_{3rm}) \cos^2 \alpha_{2rm}}$$

$$s_v = \frac{\psi_v C_{a,v}}{2(\tan \alpha_{1m} + \tan \alpha_{2m}) \cos^2 \alpha_{1m}}$$

**Number of blades/vanes :**

$$N_b = \frac{2\pi r_{m,b}}{s_b}$$

$$N_v = \frac{2\pi r_{m,v}}{s_v}$$

### 4.3.2 Geometric Results

Parameter Name	Symbol	Hub Value	Mean Value	Tip Value
Radius	$r$	84.764 mm	93.949 mm	103.135 mm
Tangential Speed	$U$	344.343 m/s	310.675 m/s	378.010 m/s
Height	$h$		18.371 mm	
Inlet Blade angle	$\beta_2$	51.635°	38.109°	19.668°
Exit Blade angle	$\beta_3$	57.590°	58.616°	59.717°
Chord Length	$C_b$		13.849 mm	
Axial Chord Length	$C_{a,b}$	13.591 mm	13.035 mm	11.967 mm
Maximum Thickness	$t_{max,b}$	3.276 mm	3.059 mm	2.759 mm
Throat Opening	$O_b$	4.244 mm	4.906 mm	5.446 mm
Leading Edge Thickness	$t_{LE}$		0.254 mm	
Trailing Edge Thickness	$t_{TE}$		0.762 mm	
Stagger Angle	$\phi_b$	11.078°	19.740°	30.222°
Zweifel Coefficient	$\psi_b$		0.95	
Pitch	$s_b$	7.916 mm	9.420 mm	10.799 mm
Number of Blades	$N_b$		63	
Tip clearance	$\Delta t_c$		0.3601 mm	

Table 4.9: Blade Geometrical results

Parameter Name	Symbol	Hub Value	Mean Value	Tip Value
Radius	$r$	84.764 mm	96.256 mm	107.749 mm
Height	$h$		22.985 mm	
Inlet Blade angle	$\beta_1$	-11.323°	-10.000°	-8.952°
Exit Blade angle	$\beta_2$	71.493°	69.645°	67.840°
Chord Length	$C_b$		45.969 mm	
Axial Chord Length	$C_{a,b}$	24.250 mm	25.716 mm	27.072 mm
Maximum Thickness	$t_{max,b}$	8.055 mm	8.024 mm	7.981 mm
Throat Opening	$O_b$	10.278 mm	11.006 mm	11.713 mm
Leading Edge Thickness	$t_{LE}$		0.508 mm	
Trailing Edge Thickness	$t_{TE}$		1.270 mm	
Stagger Angle	$\phi_b$	58.162°	55.985°	53.921°
Zweifel Coefficient	$\psi_v$		0.75	
Pitch	$s_b$	32.382 mm	31.641 mm	31.053 mm
Number of Vanes	$N_b$		19	

Table 4.10: Vane Geometrical results

### 3D geometric Presentation of stage and its components :

Based on the geometric parameters a parametric Catia model was prepared for each component of the stage:

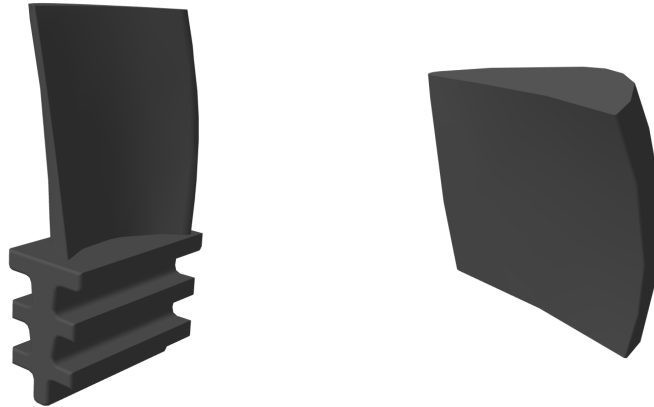


Figure 4.6: Blade and Vane 3D model

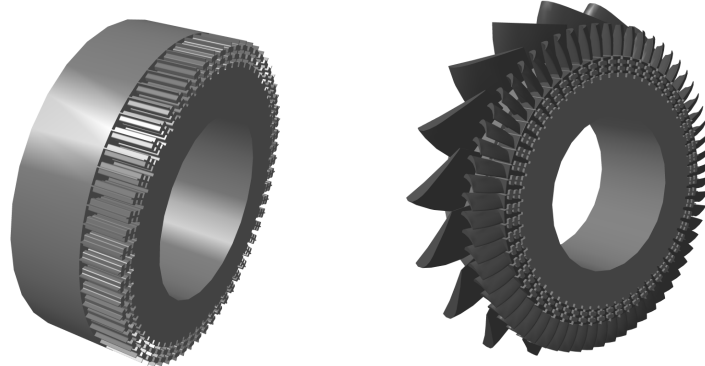


Figure 4.7: Mounting disk 3D model and stage 3D assembly model

### 4.3.3 Profile Loss

Profile loss usually arises due to the skin friction between the metal and gas along the flow-turning path. Any design decision that gives a significant metal area induces profile losses.

Profile loss coefficient can be found by using following graphs (4.8) and the relations given by Ainley and Mathieson for Turbine Profile Loss Correlation.

$$K_P = 0.914 \left( \frac{2}{3} Y_{pAMDC} K_{accel} + K_{sh} \right)$$

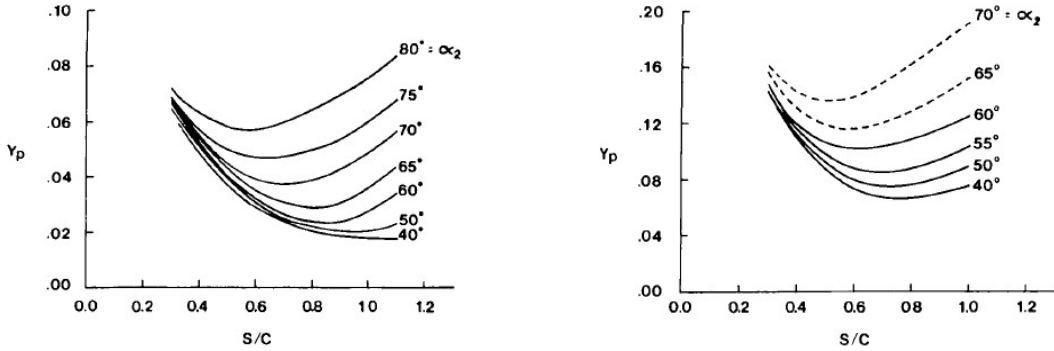


Figure 4.8: Profile loss [3]

Where,

$$Y_{pAMDC} = \left\{ Y_{p,\beta_1=0} + \left| \frac{\beta_1}{\alpha_2} \right| \left( \frac{\beta_1}{\alpha_2} \right) [Y_{p,\beta_1=\alpha_2} - Y_{p,\beta_1=0}] \right\} \left( \frac{t_{max}/C}{0.2} \right)^{\frac{\beta_1}{\alpha_2}}$$

$$K_{accel} = 1 - K_2(1 - K_1)$$

Where,

$$K_1 = 1 - 1.25(M_2 - 0.2) ; \text{ for } M_2 > 0.2$$

$$K_2 = \left( \frac{M_1}{M_2} \right)^2$$

$$K_{sh} = \frac{\Delta P}{q_{1h}} sh \frac{P_1}{P_2} \frac{\left[ 1 - \left( 1 + \frac{\gamma_g - 1}{2} M_1^2 \right)^{\frac{\gamma_g}{\gamma_g - 1}} \right]}{\left[ 1 - \left( 1 + \frac{\gamma_g - 1}{2} M_2^2 \right)^{\frac{\gamma_g}{\gamma_g - 1}} \right]}$$

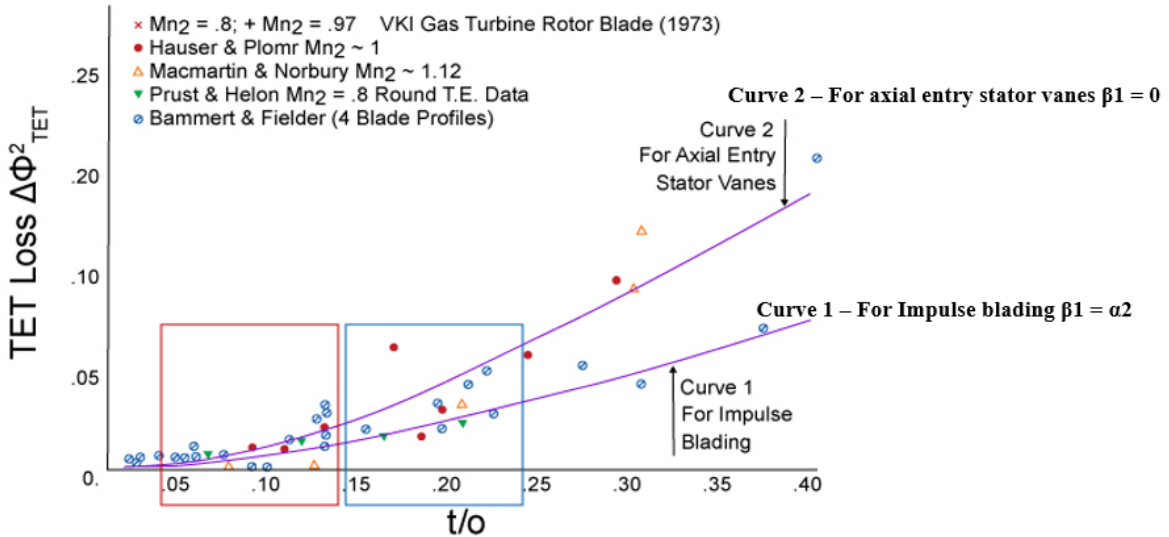
Where,

$$\frac{\Delta P}{q_{1h}} sh = \frac{r_h}{r_t} \frac{\Delta P}{q_{1h}}$$

$$\frac{\Delta P}{q_{1h}} = 0.75(M_{1h} - 0.4)^{1.75} ; \text{ for } M_{1h} > 0.4$$

#### 4.3.4 Trailing Edge Loss

When flow passes through the edge of the blade, it generates vortices and contributes to the losses. As the flow from the suction and pressure side meet at the finite trailing edge and generates trailing edge losses, it draws attention toward the trailing edge thickness of the turbine blade.


 Figure 4.9:  $TETLoss \Delta\Phi_{TET}^2$  vs  $t/o$  [3]

$$K_{TE} = \frac{\left[1 - \frac{\gamma_g - 1}{2} M_2^2 \left(\frac{1}{1 - \Delta\Phi_{TE}^2} - 1\right)\right]^{\frac{-\gamma_g}{\gamma_g - 1}} - 1}{\left[1 - \left(1 + \frac{\gamma_g - 1}{2} M_2^2\right)^{\frac{-\gamma_g}{\gamma_g - 1}}\right]}$$

Where,

$$\Delta\Phi_{TE}^2 = \Delta\Phi_{TE\beta_1=0}^2 + \left|\frac{\beta_1}{\alpha_2}\right| \left(\frac{\beta_1}{\alpha_2}\right) \left[\Delta\Phi_{TE\beta_1=\alpha_2}^2 - \Delta\Phi_{TE\beta_1=0}^2\right]$$

#### 4.3.5 Secondary Loss

Instead of passing through the flow path, flow passes through the secondary path due to a large passage between two adjacent blades. Any source of static pressure gradient that may exist that drives the mainstream air to take the secondary path drives the secondary losses.

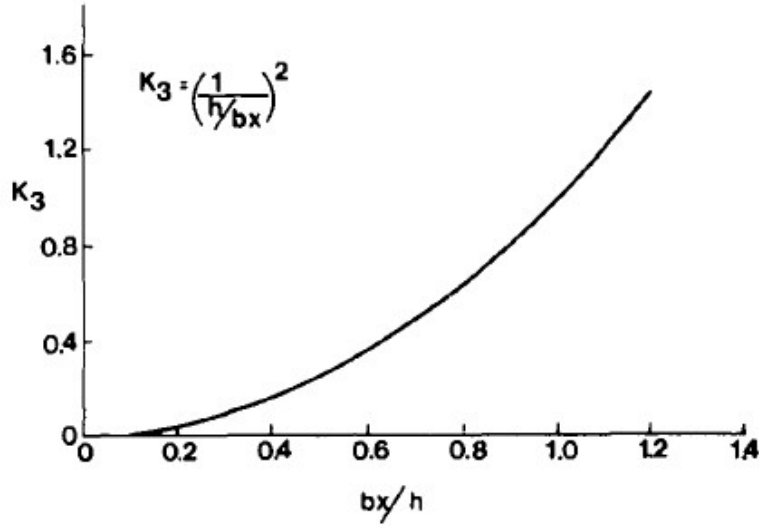


Figure 4.10: Mach number correction factor  $K_3$  for the secondary loss coefficient [3]

$$K_S = 1.2 \times Y_{s,AMDC} \times K_{cs}$$

Where,

$$K_{cs} = 1 - K_3(1 - K_{accel})$$

$$K_3 = \left(\frac{C_a}{h}\right)^2$$

$$Y_{s,AMDC} = 0.0334 f(AR) \left(\frac{\cos\alpha_2}{\cos\beta_1}\right) \left(\frac{C_L}{(s/c)}\right)^2 \left(\frac{\cos^2\alpha_2}{\cos^3\alpha_m}\right)$$

$$\frac{C_L}{(s/c)} = 2(\tan\alpha_1 - \tan\alpha_2)\cos\alpha_m$$

$$\tan\alpha_m = \frac{\tan\alpha_1 - \tan\alpha_2}{2}$$

$$f(AR) = \frac{1 - 0.25\sqrt{2 - h/c}}{h/c} ; \text{ for } h/c \leq 2$$

$$f(AR) = \frac{1}{h/c} ; \text{ for } h/c > 2$$

#### 4.3.6 Total Loss

Total loss encountered by turbine blade is the sum of all types of losses we found previously. Although, we have to take into account the effect of Mach number on profile losses. Indeed, as the flow velocity at the suction surface exceeds sonic value, the loss associated with it increases slightly due to thickening of the boundary layer through the shock waves appear in the passage region[1].

Here  $f_{Re}$  is represented by shock loss factor. Although, it is calculated based on Reynolds number of the flow i.e. formula given by D.G. Ainley, G.C.R. Mathieson

$$K_T = K_P \times f_{Re} + K_S + K_{TE} + K_{clr}$$

$$f_{Re} = \left( \frac{Re}{2 \times 10^5} \right)^{-0.4} \quad \text{for } Re \leq 2 \times 10^5$$

$$= 1.0 \quad \text{for } 2 \times 10^5 < Re < 10^6$$

$$= \left( \frac{Re}{10^6} \right)^{-0.2} \quad \text{for } Re \geq 10^6$$

### 4.3.7 Efficiency Calculation

Following, are the equations for enthalpy loss coefficient used to calculate total efficiency.

$$\zeta_R = \frac{K_{Tb}}{1 + 0.5\gamma_g M_{r3m}^2}$$

$$\zeta_N = \frac{K_{Tv}}{1 + 0.5\gamma_g M_{2m}^2}$$

$$\eta_{tt} = \frac{1}{1 + \frac{\zeta_N C_2^2 + \zeta_R V_{r3}^2}{2(h_{01} - h_{03})}}$$

### 4.3.8 Tip Clearance Loss

Flow passes through the top of the blade section instead of passing through the decided path, which creates  $u\delta v$  and results in the losses of the turbine blades. The gap between the shroud and the tip of the blade determines the contribution of tip clearance losses. The pressure difference across the blade is sensed by the flow passing through the gas path and some of the flow sneaks over the flow. The major contribution of having poor aerodynamic efficiency is having higher tip clearance loss.

Due to tip clearance loss there is an efficiency drop which is formulated below. Eventually, it gives actual efficiency at design point.

$$\Delta\eta = 0.93 \eta_0 \left( \frac{\Delta t_c}{h_b \cos \alpha_{3rm}} \right) \left( \frac{r_t}{r_m} \right)$$

$$\eta = \eta_{tt} - \Delta\eta$$

#### 4.3.9 Contribution of various losses to the overall turbine efficiency

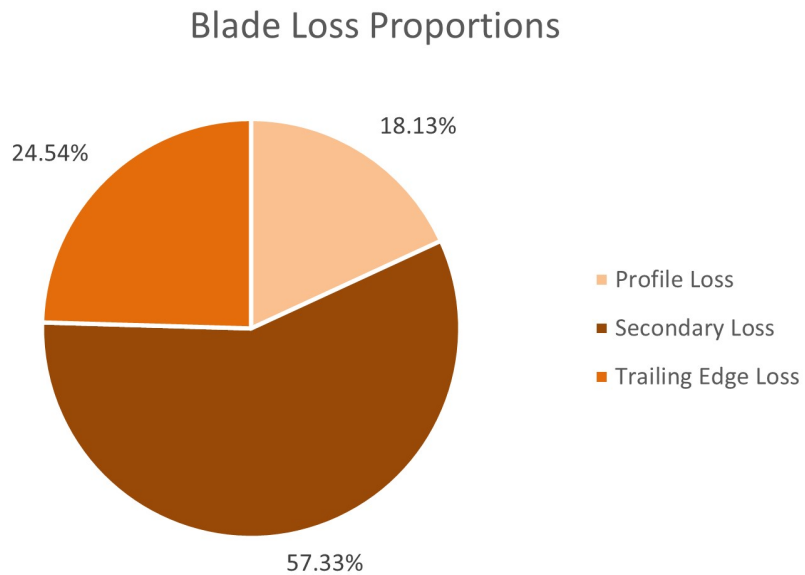


Figure 4.11: Blade losses

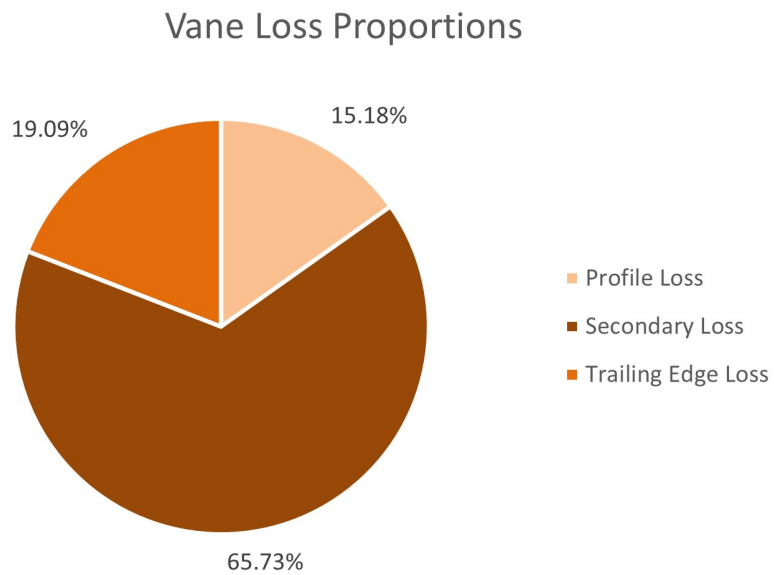


Figure 4.12: Vane losses

### 4.3.10 Final Efficiency

Parameter Name	Symbol	Value
Blade Profile Loss Coefficient	$K_{P,b}$	0.0329
Blade Secondary Loss Coefficient	$K_{S,b}$	0.1041
Blade Trailing Edge Loss Coeffient	$K_{TE,b}$	0.0446
Blade Total Loss Coeffient	$K_{T,b}$	0.1816
Vane Profile Loss Coefficient	$K_{P,v}$	0.0238
Vane Secondary Loss Coefficient	$K_{S,v}$	0.1031
Vane Trailing Edge Loss Coeffient	$K_{TE,v}$	0.0299
Vane Total Loss Coeffient	$K_{T,v}$	0.1569
Stage Efficiency	$\eta_{tt}$	84.4575%

Table 4.11: Loss coefficients and calculated efficiency

From Iterative process and changing the ranges for various parameters we got the final stage efficiency at design point as below :

$$\eta_{tt} = 84.4575\%$$

## 4.4 Off-Design Calculations

In turbine design, "off-design" refers to conditions or operating points that are different from the design point for which the turbine was optimized. Off-design conditions can occur due to variations in parameters or reduction in rotational speed.

### 4.4.1 Assumptions

- Mass flow rate is same as design conditions
- Vane exit properties stay the same as design conditions
- Blade exit relative flow angle stays the same as design conditions
- 10% reduction in speed constitutes to 10% reduction in work done

### 4.4.2 Calculating Incidence Angle

Reduction in RPM by 10 % leads to reduction in work output. This criteria for off-design results in calculation of all the dependent parameters which is formulated below.

$$N_i = 0.90 \times N$$

$$W_{HPTi} = 0.90 \times W_{HPT}$$

$$T_{03i} = T_{01} - \frac{W_{HPTi}}{Cp_g}$$

Off-design calculations in turbine design often result in alterations to the velocity triangles at both the inlet and exit of the turbine blades. These changes occur due to variations in operating conditions from the turbine's design point.

$$U_{mi} = \frac{2\pi r_{m,b} N_i}{60}$$

$$V_{w2mi} = C_{w2m} - U_{mi}$$

$$V_{2mi} = \sqrt{C_{a2m}^2 + V_{w2mi}^2}$$

$$\tan\alpha_{2rmi} = \frac{V_{w2mi}}{C_{a2m}}$$

$$M_{2rmi} = \frac{V_{2mi}}{\sqrt{\gamma_g R_g T_2}}$$

$$C_{w3mi} = \frac{W_{HPTi}}{U_{mi}} - C_{w2}$$

$$V_{w3mi} = C_{w3mi} + U_{mi}$$

$$C_{a3mi} = \frac{V_{w3mi}}{\tan\alpha_{3rm}}$$

$$C_{3mi} = \sqrt{C_{a3mi}^2 + C_{w3mi}^2}$$

$$\tan\alpha_{3mi} = \frac{C_{w3mi}}{C_{a3mi}}$$

$$V_{3mi} = \sqrt{C_{a3mi}^2 + V_{w3mi}^2}$$

$$T_{3mi} = T_{03i} - \frac{V_{3mi}^2}{2Cp_g}$$

$$M_{3rmi} = \frac{V_{3i}}{\sqrt{\gamma_g R_g T_{3i}}}$$

$$M_{3mi} = \frac{C_{3i}}{\sqrt{\gamma_g R_g T_{3i}}}$$

The alteration in velocity triangles results in a modification of the incidence angle at the inlet of the turbine blade. This angle, crucial for turbine performance analysis, is determined by the following formula:

$$i = \alpha_{2rmi} - \beta_2$$

The incidence angle represents the angle between the relative velocity vector and the chord line of the blade. It plays a significant role in determining the aerodynamic performance of the turbine blade. By tracking changes in the incidence angle under off-design conditions, engineers can assess the impact on turbine efficiency and make necessary adjustments to optimize performance across a range of operating conditions.

#### 4.4.3 Results from Mean Line Analysis

The below results are at 10% less speed than design point, which is  $N_i = 31,500 \text{ RPM}$ :

Parameter Name	Symbol	Value
Mach Number - 1	$M_{1i}$	Same as before 0.1250
Absolute Velocity - 1	$C_{1i}$	Same as before 86.394 m/s
Axial Velocity - 1	$C_{a1i}$	Same as before 85.082 m/s
Tangential Velocity - 1	$C_{w1i}$	Same as before -15.002 m/s
Absolute Flow Angle - 1	$\alpha_{1i}$	Same as before -10.000°
Static Temperature - 1	$T_{1i}$	Same as before 1248.642 K
Static Pressure - 1	$P_{1i}$	Same as before 1169.784 kPa
Total Temperature - 1	$T_{01i}$	Same as before 1251.890 K
Total Pressure - 1	$P_{01i}$	Same as before 1182.014 kPa
Mach Number - 2	$M_{2i}$	Same as before 0.7929
Absolute Velocity - 2	$C_{2i}$	Same as before 518.017 m/s
Axial Velocity - 2	$C_{a2i}$	Same as before 180.185 m/s
Tangential Velocity - 2	$C_{w2i}$	Same as before 485.669 m/s
Absolute Flow Angle - 2	$\alpha_{2i}$	Same as before 69.645°
Static Temperature - 2	$T_{2i}$	Same as before 1115.457 K
Static Pressure - 2	$P_{2i}$	Same as before 793.223 kPa
Total Temperature - 2	$T_{02i}$	Same as before 1231.330 K
Total Pressure - 2	$P_{02i}$	Same as before 1182.014 kPa
Mach Number - 3	$M_{3i}$	0.5351
Absolute Velocity - 3	$C_{3i}$	322.628 m/s
Axial Velocity - 3	$C_{a3i}$	283.26 m/s
Tangential Velocity - 3	$C_{w3i}$	154.442 m/s
Absolute Flow Angle - 3	$\alpha_{3i}$	28.600°
Static Temperature - 3	$T_{3i}$	950.231 K
Static Pressure - 3	$P_{3i}$	442.728 kPa
Total Temperature - 3	$T_{03i}$	1079.089 K
Total Pressure - 3	$P_{03i}$	533.460 kPa

Table 4.12: Mean line absolute results at Off-design conditions

Parameter Name	Symbol	Value
Relative Mach Number - 2	$M_{2ri}$	0.3853
Relative Velocity - 2	$V_{2i}$	251.711 m/s
Relative Tangential Velocity - 2	$V_{w2i}$	175.761 m/s
Relative Flow Angle - 2	$\alpha_{2ri}$	44.288°
Total Relative Temperature - 2	$T_{02ri}$	1143.052 K
Total Relative Pressure - 2	$P_{02ri}$	874.679 kPa
Relative Mach Number - 3	$M_{3ri}$	0.9021
Relative Velocity - 3	$V_{3i}$	543.728 m/s
Relative Tangential Velocity - 3	$V_{w3i}$	464.350 m/s
Relative Flow Angle - 3	$\alpha_{3ri}$	Same as before 58.616°
Total Relative Temperature - 3	$T_{03ri}$	1079.089 K
Total Relative Pressure - 3	$P_{03ri}$	736.308 kPa

Table 4.13: Mean line relative results at Off-design conditions

Parameter Name	Symbol	Hub Value	Mean Value	Tip Value
Blade Tangential Speed	$U_i$	279.608 m/s	309.908 m/s	340.209 m/s
Absolute Flow Angle - 3	$\alpha_{3i}$	28.600°	31.145°	26.412°
Relative Flow Angle - 2	$\alpha_{2ri}$	55.142°	44.288°	29.563°
Incidence	$i$	3.507°	6.179°	9.894°

Table 4.14: Other Off-design parameters at hub, mean and tip

#### 4.4.4 Off-Design Profile Loss Calculations

When calculating profile losses at off-design conditions, a similar approach is employed as in the previous discussion. However, particular attention is paid to the alteration in blade angles. The formula remains consistent, but with adjustments to account for changes in blade angles.

Off-design condition doesn't affect much to the profile loss, although profile loss slightly increases due to changes in inlet gas angle.

$$\Phi_{P0}^2 = \frac{1}{1 + \frac{K_p}{K_1 + K_2 K_p}}$$

$$(d/s)^{-1.6} \times \left( \frac{\cos\beta_1}{\cos\beta_2} \right)^{-2} \times i$$

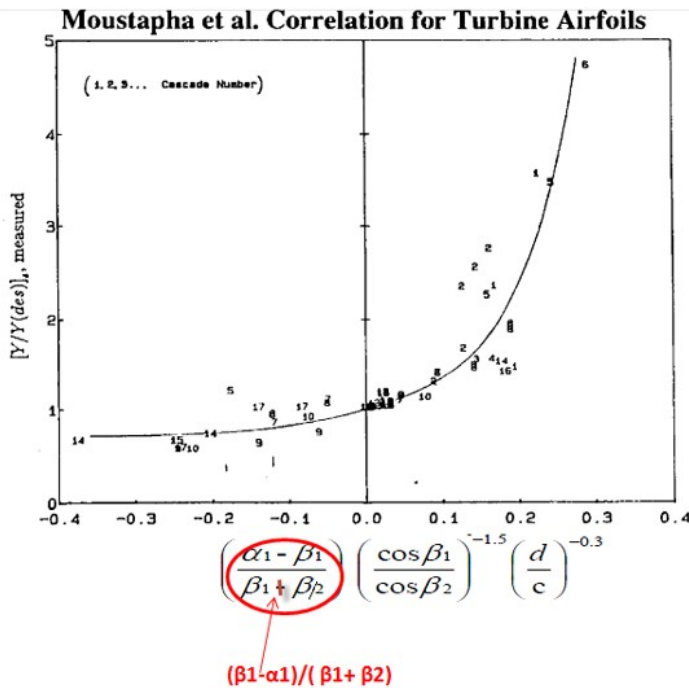


Figure 4.13: Effect of incidence on profile loss [4]

$$\Phi_P^2 = \Phi_{P0}^2 - \Delta\Phi_{INC-P}^2$$

$$K_p = \frac{K_1 (1 - \Phi_P^2)}{\Phi_P^2 - K_2 (1 - \Phi_P^2)}$$

#### 4.4.5 Off-Design Secondary Loss Calculations

When calculating secondary loss at off-design conditions, the similar methodology is followed as employed in the previous section.

Change in inlet gas angle leads to a tremendous increase in secondary loss as gas flow deviates from the flow path and that would increase the secondary losses. Thus, increase in secondary losses at off-design gives a drop in overall turbine efficiency at off-design conditions.

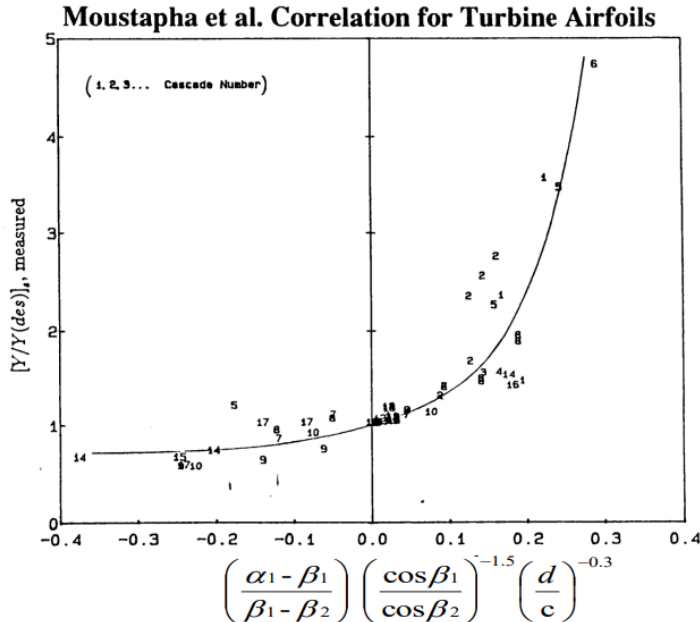


Figure 4.14: Effect of incidence on secondary loss [4]

Calculate :

$$\left( \frac{\alpha_1 - \beta_1}{\beta_1 + \beta_2} \right) \left( \frac{\cos \beta_1}{\cos \beta_2} \right)^{-1.5} \left( \frac{d}{C} \right)^{-0.3}$$

From the figure 4.14 we can find the  $\left( \frac{K_s}{K_{s,des}} \right)$

#### 4.4.6 Off-Design Trailing Edge Loss Calculations

The procedure to calculate the trailing edge loss remains the same as the design condition. However, the values used will be based on the values we got with the incidence.

$$K_{TE} = \frac{\left[ 1 - \frac{\gamma_g - 1}{2} M_{2i}^2 \left( \frac{1}{1 - \Delta \Phi_{TEi}^2} - 1 \right) \right]^{\frac{-\gamma_g}{\gamma_g - 1}} - 1}{\left[ 1 - \left( 1 + \frac{\gamma_g - 1}{2} M_{2i}^2 \right)^{\frac{-\gamma_g}{\gamma_g - 1}} \right]}$$

#### 4.4.7 Contribution of various losses to the overall turbine efficiency at Off-design conditions

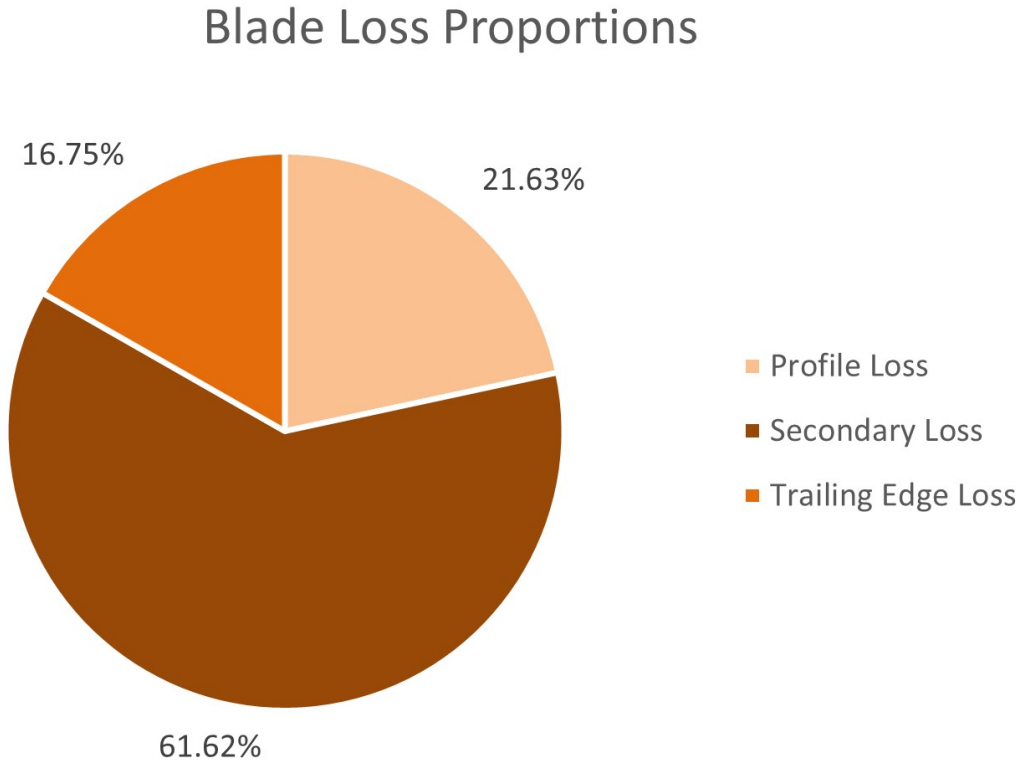


Figure 4.15: Off-design blade losses

#### 4.4.8 Off-Design Efficiency Calculations

Parameter Name	Symbol	Value
Blade Profile Loss Coefficient	$K_{P,b}$	0.0525
Blade Secondary Loss Coefficient	$K_{S,b}$	0.1496
Blade Trailing Edge Loss Coeffient	$K_{TE,b}$	0.0407
Blade Total Loss Coeffient	$K_{T,b}$	0.2428
Vane Profile Loss Coefficient	$K_{P,v}$	Unchanged : 0.0238
Vane Secondary Loss Coefficient	$K_{S,v}$	Unchanged : 0.1031
Vane Trailing Edge Loss Coeffient	$K_{TE,v}$	Unchanged : 0.0299
Vane Total Loss Coeffient	$K_{T,v}$	Unchanged : 0.1569
Stage Efficiency	$\eta_{tt,i}$	80.5914%

Table 4.15: Off-Design loss coefficients

From the data filtration process and the main condition being efficiency above 83.00%, the filtered data was then again tested with the off-design performance through the process shown above. We checked the off-design performance and selected the final data for which all the values were shown. Also, while calculating the off-design performance, the efficiency we derived was :  $\eta_{tt,i} = 80.5914\%$

#### 4.4.9 Stress Calculation

As each rotor airfoil cross-sectional area needs to limit the centrifugal force on all of the material outside of its radial location, the hub or base of the airfoil needs to exert the most force [5].  $A_h$  is subject to a total centrifugal force so that the principal tensile stress is given by :

$$\sigma_c = \frac{\rho\omega^2 A_{an}}{4\pi} \left( 1 + \frac{A_t}{A_h} \right)$$

$$\sigma_c = 172.993 \text{ MPa}$$

## Chapter 5

# PART D - HPT DESIGN TRADE STUDIES

### 5.1 Trade study of HPT factory standard cost vs. stage efficiency

In this section, we will present a trade study of HPT factory standard cost depending on different material and the consequences on stage efficiency.

Knowing that the lifespan of a helicopter engine is estimated at 25,000 hours, and the average use of such an engine is about 2,500 hours per year, this gives a product lifespan of 10 years. Additionally, such an engine requires multiple maintenances over its lifespan (in order to ensure the safety of all users) requiring the change of all the blades and vanes. The following table presents all the costs incurred by maintenance visits over the life of the engine from the different proposed materials and their characteristics.

MATERIAL	MATERIAL CHARACTERISTICS		OVERHAUL VISITS		TOTAL OVERHAUL COST
	Sell price	Lifetime (hr)	Number	Total cost	
X	15120.00 \$	5000	5	450000.00\$	525600.00 \$
Y	12600.00 \$	4000	6	540000.00 \$	615600.00 \$
Z	15120.00 \$	8000	3	270000.00\$	322920.00 \$

Table 5.1: Cost of material and overhaul visits

Figure 5.1 presents the evolution of the efficiency (at 35,000 RPM) depending on FSC for each material :

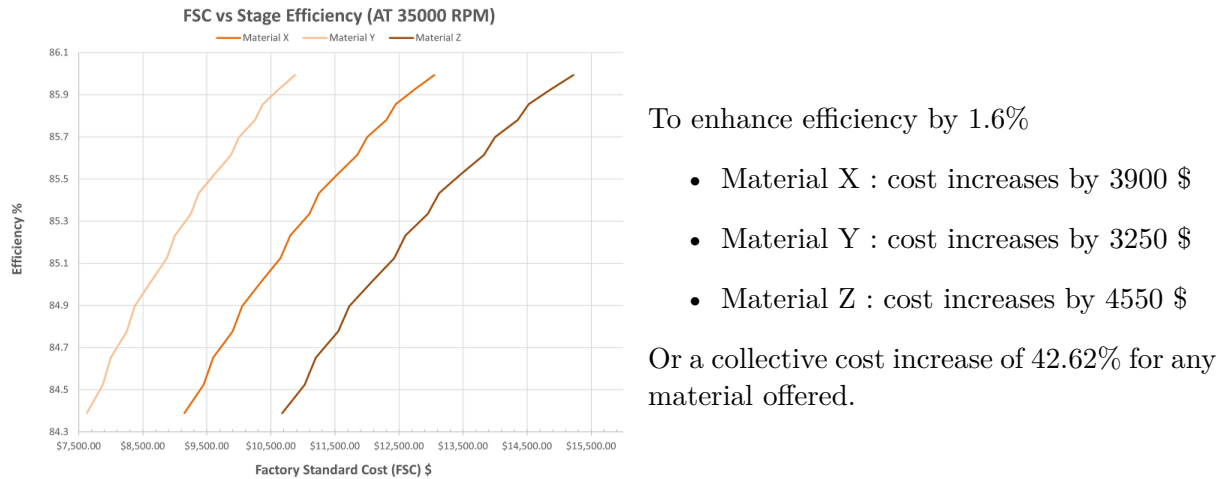


Figure 5.1: FSC vs Stage efficiency

Thus, although material Z involves a higher purchase cost to the customer, with a long-term view, this purchase cost is largely offset by the maintenance cost and also offers better quality.

## 5.2 Engine weight reduction

In this section, we focus on reducing the engine's weight, which brings several significant benefits, whether they be economic, environmental or technical :

- **Improvement in energy efficiency** : A lighter engine plays a crucial role in enhancing a vehicle's or any other motorized device's energy efficiency. By reducing weight, the engine needs to exert less effort to propel or operate the device, resulting in lower specific fuel consumption. This reduction in fuel consumption also leads to a significant decrease in CO<sub>2</sub> emissions and other atmospheric pollutants. For businesses and consumers concerned about their environmental impact, this increased efficiency represents a major advantage.
- **Increased performance** : Lightening the engine has a direct impact on the device's performance. Indeed, this can result in better maneuverability and increased stability, which is particularly important for high-performance vehicles. A reduction in weight also allows for improved acceleration and the vehicle's ability to carry more. For a helicopter, this might mean the ability to increase payload or achieve longer distances without refueling.
- **Lower operating costs** : A lighter and more efficient engine can lead to reduced operating costs. The decrease in fuel consumption translates into substantial savings on fuel, especially when its price is high or fluctuates. Moreover, a lighter engine can result in reduced wear on other vehicle components, such as brakes and tires, thereby reducing maintenance and servicing costs in the long term.
- **Reduced wear on components** : By reducing the engine weight, the stress imposed on the entire vehicle or device is decreased. Less weight means less strain on mechanical components, reducing wear and extending their lifespan. This is particularly relevant for components that are costly to replace or repair. Consequently, users benefit from longer periods between maintenance and increased device reliability.

In order to reduce the engine weight, it is necessary to consider an increase in the maximum temperature of the cycle. However, for each increase of 100°F in peak cycle temperature, the

HPT cooling consumption must increase by 1% of Combustor exit mass flow and this cooling flow increase in turn reduces the HPT efficiency by 0.2%.

We can then establish the evolution of the engine weight as well as the efficiency in relation to this increase in peak cycle temperature, which yields the following graph :

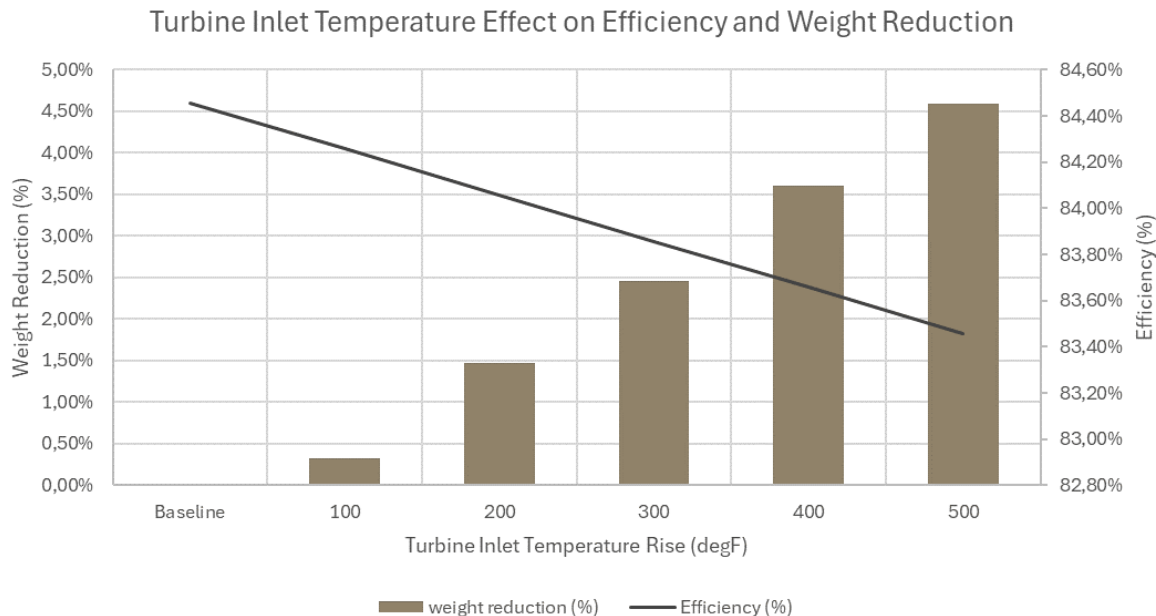


Figure 5.2: Turbine inlet temperature effect on efficiency and weight reduction

From an SFC point of view, we notice that, by increasing the temperature at the turbine inlet, this implies a reduction in the number of blades required. However, it also increases the engine's fuel consumption as show following graphs:

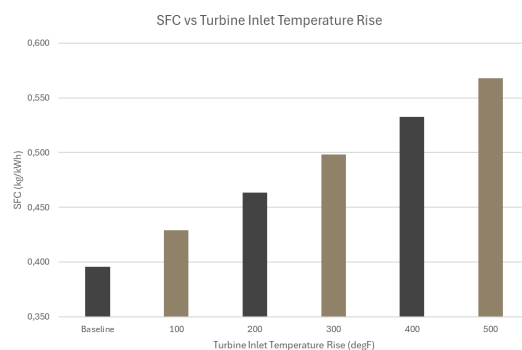


Figure 5.3: SFC vs. Turbine inlet temperature rise

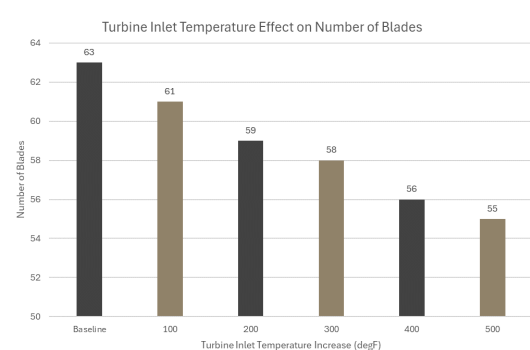


Figure 5.4: Turbine temperature inlet effect on number of blades

Although an increase in cycle temperature could lead to higher SFC, we must balance this with the trade-off in stage efficiency to optimize performance.

Temperature Rise (def F)	Total fuel cost for Z (\$)	Change (%)
Baseline	8295	Baseline
100	8998	7.82
200	9718	7.40
300	10441	6.93
400	11170	6.52
500	11903	6.16

Table 5.2: Evolution of fuel cost depending on temperature rise

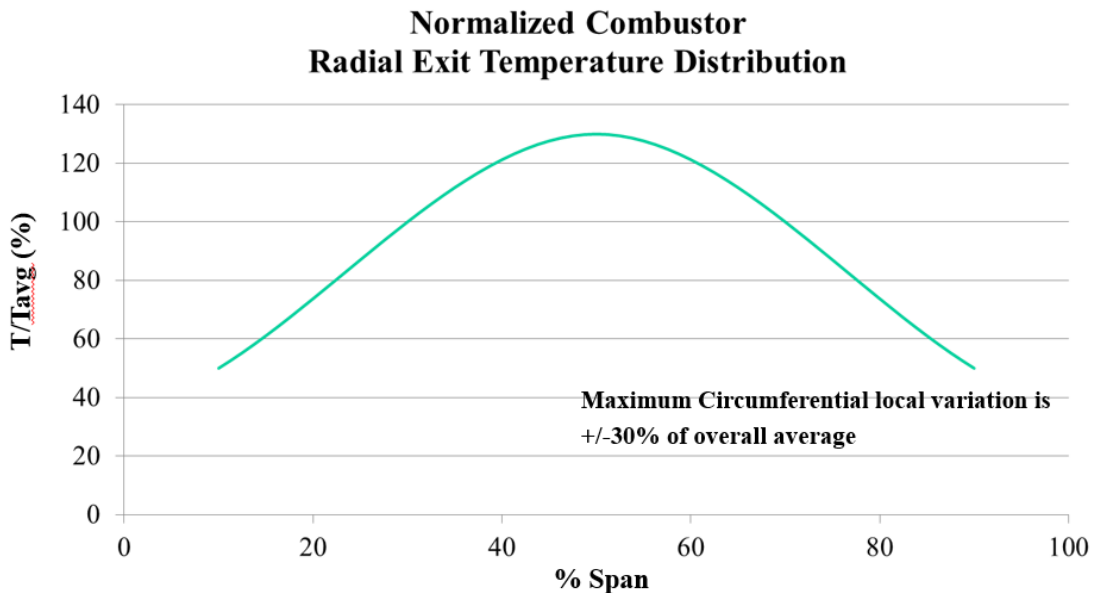


Figure 5.5: Normalized temperature distribution curve

We also have to consider the normalized temperature distribution curve for the gases coming from the combustor. The selected material should be capable of taking the hot gases coming from the combustor. From the 5.5 it can be seen that at the 50% of span temperature would be 20% higher than the mean temperature.

$$\frac{T_{max}}{T_{avg}} = 1.3$$

$$T_{avg} = 1626 \text{ K}$$

So, if we have to consider weight reduction by increasing 100° F then the mean temperature along the combustor exit is 1306.51 K. Which eventually gives the maximum temperature of 1698.51 K. Therefore, an increase in cycle temperature for reduction in weight draws attention towards the maximum temperature that turbine vane has to face, which also deteriorate life of the turbine blade.

### 5.3 5 years technology plan

Nowadays, the industry must strive to invest in reducing its carbon footprint. In the aerospace field, this effort is largely made through fuel consumption.

Indeed, the latest generations of aircraft currently in service are certified to operate with up to 50% biofuel. However, the level of production does not allow, by far, to reach this rate today, and the available biofuels are primarily first-generation biofuels. First-generation biofuels are essentially produced from plant seeds, either oilseed (rapeseed, sunflower) or cereal-based (ethanol from wheat or corn). The aviation sector, however, targets the use of second-generation biofuels and beyond. Their main advantage over the first generation is that their production significantly reduces competition for agricultural land, habitable or forest areas. They are synthesized, for example, from forest, agricultural, or municipal waste.

Another alternative solution is Power-to-Liquid (PTL) fuels, which are synthetic fuels that can be produced from CO<sub>2</sub> and hydrogen (H<sub>2</sub>). CO<sub>2</sub> can be obtained by capture in the air or from production area outputs (factory emissions, for example). While this technology seems particularly attractive from the standpoint of decarbonization, its climate impact depends on the implementation processes, particularly the carbon neutrality of the energy used for the synthesis of PTLs and, upstream in the chain, of the hydrogen.

Biofuels and PTLs have the advantage of being 'drop-in,' meaning they require little or no modifications to existing engines and aircraft. This presents a real advantage since future innovations and improvements can thus be compatible with our current engines. The decarbonizing power of biofuels and PTLs is not expressed during combustion, which emits as much as kerosene. It comes from the upstream CO<sub>2</sub> absorption necessary for their production and their manufacturing process. Thus, the real decarbonization related to the use of these alternative energies can only be assessed by looking at the complete life cycle, from manufacturing to combustion in flight.

Diagram 5.6 presents a 5-year development plan for these solutions to reduce its environmental impact :

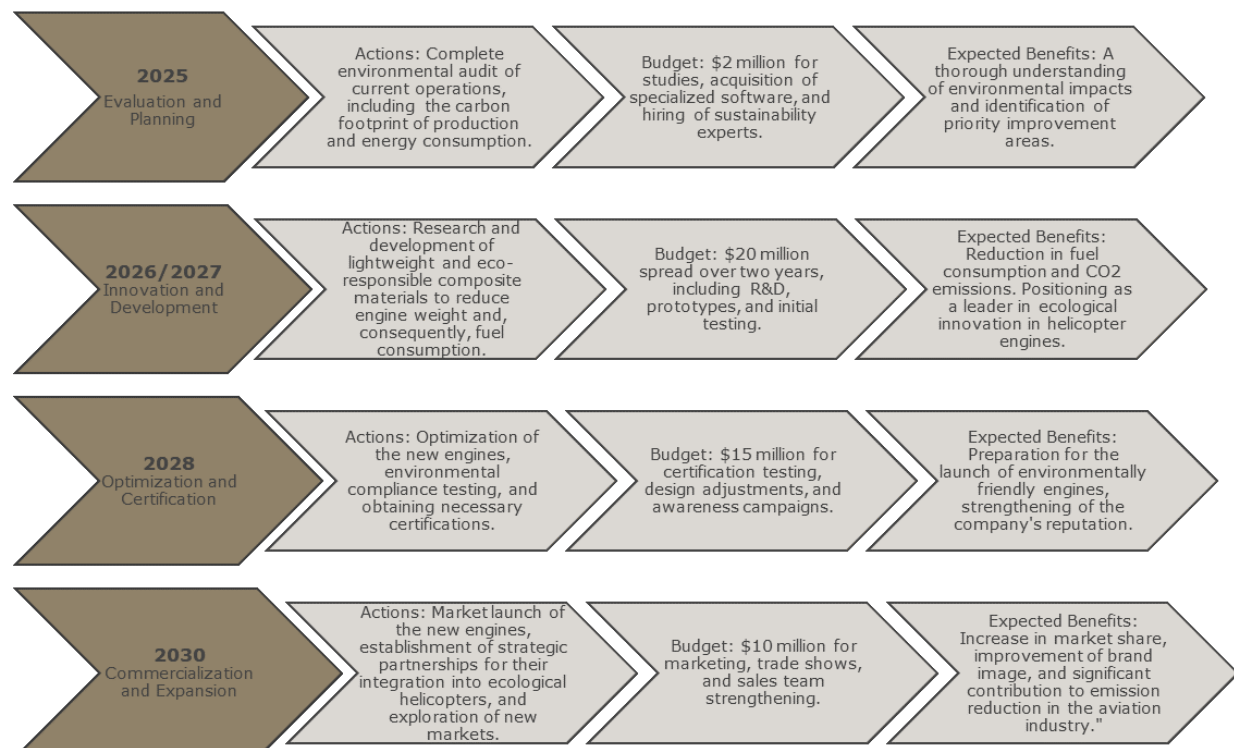


Figure 5.6: 5 years technology plan

Similarly, many actions can also be integrated into daily life such as waste reduction, recycling, and optimizing energy consumption in facilities. Additionally, the plan involves training and raising awareness among employees through a continuous education program on sustainable practices and technological innovations. To successfully implement this plan, various partnerships could be established, allowing the industry to develop more rapidly. This will include collaborations with universities, research institutes, and other companies to share knowledge and co-develop green technologies.

This carbon footprint reduction plan requires a total planned investment of \$47 million over five years. The Government of Quebec has recently committed to providing financial support for collaborative and mobilizing projects on the development of tomorrow's transportation technologies. The company also anticipates a decrease in the cost of Sustainable Aviation Fuels (SAFs) in the coming years due to their production and commercialization on a larger scale, improvements in manufacturing technologies, and increased support from governments and financial institutions. This will enable the company to become profitable following the commercialization of our engines within 5 years. The expected benefits include not only a significant positive impact on the environment but also a sustainable competitive advantage through innovation and improved brand image.

## 5.4 Introducing two additional derivative engines into the market

The introduction of a new family of helicopter engines, achieved by adding two additional engines offering +10% and -10% power respectively, each with a common core, provides the company with several significant advantages, both technical and economic.

**The main advantages of this strategy include :**

- Significant savings : By standardizing certain components, we ensure reduced production costs in the design of similar engines, thereby guaranteeing performance. The production of new engines is thus more efficient and economical.
- Wide market flexibility : Offering engines of different powers allows P&W to target a larger market share by meeting more needs and applications.
- Reduced R&D costs : By designing a single technology for the core, it allows for the consolidation of research efforts on new innovations and improvements that can be applied across the entire engine family.
- Provides good brand recognition and more efficient manufacturing

**Technical trade-offs :**

- Performance optimization : Adapting each major component to operate efficiently at different powers requires compromises, such as adjusting the geometry of components or changing materials to meet varying thermal or mechanical constraints.
- Temperature management : Variations in power demand can pose challenges in terms of thermal management, potentially necessitating more sophisticated cooling systems or materials capable of withstanding higher temperatures.
- Maintenance complexity : While the common core may simplify some aspects of maintenance, differences between derived engines may introduce complexity into maintenance procedures and the training required for technicians.

- Cost trade-off with power output due to material constraint.

**Mitigating technical trade-offs :**

- Modular technologies: Adopting a modular design approach when possible, allowing for easy customization of engines for different powers while maintaining a common base.
- Advanced materials: Using lightweight composite materials and heat-resistant superalloys can help manage temperature and pressure variations while minimizing impact on weight and durability.
- Advanced simulation and modeling : Use simulation tools to predict and optimize component performance across different engine configurations, allowing for the identification and resolution of compromises before production.

# Chapter 6

## Limitations and Conclusion

### 6.1 Limitations

- Uncertainty about the material choices as we have limited technical data available.
- The analysis of off-design performance for the turbine and compressor blades may not fully capture all potential off-design scenarios or operating conditions. Variability in operational parameters, such as ambient temperature, altitude, or fuel composition, could impact engine performance differently than anticipated.
- While mathematical modelling techniques and Python code are used for optimization, the validation of these models against experimental data or real-world performance tests may be limited. Without robust validation, there could be discrepancies between predicted and actual performance.
- For stress calculations, only centrifugal stresses have been considered. Although, there are thermal stresses which affects the overall life of the turbine blade.
- While the 5-year technological business plan demonstrates commitment to growth and innovation, it may overlook external factors such as market fluctuations, regulatory changes, or competitive pressures. Adapting to unforeseen challenges or disruptions could require flexibility and agility in execution.

### 6.2 Conclusion

In conclusion, the design and optimization efforts undertaken in this study have yielded promising results in enhancing the efficiency and performance of the high-pressure turbine (HPT) within the gas turbine engine. Despite falling slightly short of the targeted efficiency of 85 percent, the achieved efficiency of 84.59 percent signifies significant progress towards meeting performance goals.

Moreover, the comprehensive analysis of off-design criteria for the HPT provides valuable insights into the engine's performance across varying operating conditions. This thorough examination ensures that the engine maintains robustness and reliability, even under non-standard operating scenarios.

As we continue to pursue advancements in gas turbine technology, it is imperative to acknowledge the iterative nature of design and optimization processes. While the current results are promising, ongoing refinements and improvements will be necessary to further enhance performance and meet evolving industry demands.

## Chapter 6. Limitations and Conclusion

---

In addition, the presentation of a 5-year technological business plan underscores our organization's commitment to continuous growth and future-oriented innovation. By aligning our objectives with the expectations of our partners, such as Pratt & Whitney, we aim to drive sustained progress and deliver exceptional value in the realm of aerospace engineering.

Overall, the findings presented in this study lay a solid foundation for further advancements in gas turbine engine design and development, positioning us at the forefront of innovation in the aerospace industry.

# Bibliography

- [1] D.G. Ainley, G.C.R. Mathieson, and Great Britain. Her Majesty's Stationery Office. *Examination of the Flow and Pressure Losses in Blade Rows of Axial-flow Turbines*. ARC technical report. H.M. Stationery Office, 1951.
- [2] S.L. Dixon and C.A. Hall. Chapter 6 - three-dimensional flows in axial turbomachines. In S.L. Dixon and C.A. Hall, editors, *Fluid Mechanics and Thermodynamics of Turbomachinery (Seventh Edition)*, pages 215–263. Butterworth-Heinemann, Boston, seventh edition edition, 2014.
- [3] S. C. Kacker and U. Okapuu. A Mean Line Prediction Method for Axial Flow Turbine Efficiency. *Journal of Engineering for Power*, 104(1):111–119, 01 1982.
- [4] A. J. Main, M. L. G. Oldfield, G. D. Lock, and T. V. Jones. Free Vortex Theory for Efficiency Calculations From Annular Cascade Data. *Journal of Turbomachinery*, 119(2):247–255, 04 1997.
- [5] J.D. Mattingly, W.H. Heiser, D.T. Pratt, American Institute of Aeronautics, and Astronautics. *Aircraft Engine Design, Second Edition*. AIAA education series. American Institute of Aeronautics and Astronautics, 2002.
- [6] H. I. H. Saravanamuttoo, G. F. C. Rogers, H. Cohen, and P. V. Straznicky. *Gas Turbine Theory*. Pearson Prentice Hall, Harlow, England; New York, 6 edition, 2009.
- [7] Y. R. Tsukasa. *Handbook of Centrifugal Compressor Design (Course Material)*. Concordia University, Montreal, 2024.